



# **Dynamic Stability of Pile Foundations Under Seismic Excitations with Two Frequencies**

Sina Behboudi

*A thesis submitted to Faculty of Graduate Studies  
in partial fulfillment of the requirements for the  
Degree of Master of Science in Civil Engineering*

Supervisor: **Dr. Jian Deng**

Chair and Associate Professor, Dept. of Civil Engineering

Co-Supervisor: **Dr. Hao Bai**

Associate Professor, Dept. of Mechanical Engineering

Lakehead University, Thunder Bay, ON, Canada

May 2024

## **Author Declaration**

I declare that I am the sole author of this thesis. This is the final version, including any required revisions, as accepted by my examiners. I understand that my thesis may be made public electronically.

## Abstract

In civil engineering, deep foundation systems, specifically pile foundations, play a critical role in transferring the structural loads of heavy constructions from superstructures to deeper layers of soil. The consequences of such failures are far-reaching and can incur property damage, structural failure, and tragically, loss of human lives. It is imperative to address the potential risks associated with pile foundation failure, particularly under seismic conditions. Conventionally only dynamic forces with a single frequency are investigated. In many cases of Civil Engineering, however, the dynamic force is not periodic with a single frequency but quasi-periodic with multiple frequencies. While there have been numerous studies on the buckling stability of piles, there is a noticeable scarcity of research that considers the influence of seismic excitations with two frequencies.

The primary objective of this research is to study the dynamic stability of pile foundations under seismic excitations with two frequencies analytically and numerically. The study commences by deriving the equation of motion for a pile foundation under earthquake, which is decoupled into an ordinary differential equation with variable coefficients of two frequencies. The harmonic balance method is used to analytically construct the stability diagrams of the pile. A numerical method is also presented to study the stability of columns under dynamic loads with two frequencies. The numerical results of instability diagrams can also serve as a calibration of other approximate results. As an application example, the dynamic stability of a real pile foundation is investigated using both the harmonic balance method and the numerical method. This is followed by parametric studies involving factors such as elastic foundation rigidity, damping, and dynamic and static loads on the instability regions. The outcomes of this research carry significant practical implications, particularly in the domain of designing pile foundations for mega-structures. Designers can leverage the findings of this study to incorporate the effects of multiple frequencies on pile behavior into their design considerations, thereby enhancing the structural age and safety of constructions.

**Keywords:** Pile Foundation, Seismic Excitations with Two Frequencies, Stability Diagram, Quasi-Periodic Mathieu Equation, Harmonic Balance Method, Numerical method

## Acknowledgment

I extend my deepest appreciation to Dr. Jian Deng, my supervisor, for granting me the opportunity to pursue further education and for providing unwavering support, patience, motivation, and valuable suggestions throughout the completion of the thesis. I also want to express gratitude to Dr. Hao Bai, my co-supervisor, for his encouragement and assistance during this academic program.

My sincere thanks go to thesis committee members, Dr. Mohammed El-Gendy and Dr. Wilson Wang, for dedicating his time to review my work. His valuable suggestions and insights significantly improved the quality of my research and also my sincere thanks go out to the session chair, Dr. Liang Cui.

I express heartfelt gratitude to my dear friend, Mohammadmehdi Shahroudi, for his active cooperation, kind counsel, and invaluable assistance in the writing of this dissertation.

A special acknowledgment goes to my supportive Mother, Rabeeh, for her unwavering encouragement throughout my life. I extend sincere thanks to my friends whose motivation sustained me over these two years.

In conclusion, I want to underscore the profound impact of the financial support I've received. The Natural Sciences and Engineering Research Council of Canada (NSERC) [RGPIN 2019 06069] and the Government of Canada's New Frontiers in Research Fund (NFRF) [NFRFR-2021-00262] have played a pivotal role, and I am deeply appreciative. Equally significant is the invaluable backing from Lakehead University, through the Graduate Assistantship, Faculty Award, and Entrance Award, which has empowered and enriched my academic pursuit in a truly impactful way.

*This thesis is dedicated to my mother, Rabeeh, whose profound influence has shaped my growth and development.*

## Table of Content

<b>Author Declaration</b> .....	<b>i</b>
<b>Abstract</b> .....	<b>ii</b>
<b>Acknowledgment</b> .....	<b>iii</b>
<b>Table of Content</b> .....	<b>v</b>
<b>Table of Figures</b> .....	<b>viii</b>
<b>Abbreviations</b> .....	<b>ix</b>
<b>Chapter 1 Introduction</b> .....	<b>1</b>
1.1 Introduction .....	1
1.2 Pile's Purposes .....	1
1.2.1 A Synopsis of the Role of Pile .....	2
1.2.2 Typical Functions of Piles .....	3
1.3 A System of Classifying Piles .....	3
1.4 Pile Foundation Excited by Seismicity .....	4
1.4.1 Earthquake-Related Pile Behavior .....	4
1.4.2 Pile's Failure Types .....	6
1.5 Research on Pile Foundation Buckling Instability .....	7
1.6 Dynamic stability of constructions undergoing quasi-periodic frequency .....	10
1.6.1 The objective of employing Quasi-Periodic Waves in Structural Design to Model Seismic Dynamic Loads .....	10
1.6.2 Study on Quasi-Periodic and Its Application Rationale .....	12
1.6.3 Research on dual-frequency excitation in the realm of civil engineering .....	13
1.7 Quasi-Periodic Hill Equation and Related Work .....	16
1.8 Building the Basis with an Elastic Pile Modelling .....	17
1.9 Thesis Outline .....	20

1.10 Summary.....	21
<b>Chapter 2 A Model of Pile Foundations Under Seismic Excitations.....</b>	<b>22</b>
2.1 Introduction .....	22
2.2 Problem formulation.....	22
2.2.1 Dynamic load with one frequency .....	26
2.2.2 Dynamic load with two frequencies .....	27
2.3 Summary.....	29
<b>Chapter 3 Dynamic Stability by Approximate Method.....</b>	<b>30</b>
3.1 Introduction .....	30
3.2 Dynamic Stability by Harmonic Balance Method.....	30
3.3 Summary.....	35
<b>Chapter 4 Dynamic Stability by Numerical Method .....</b>	<b>36</b>
4.1 Introduction .....	36
4.2 The importance of using the numerical method. ....	36
4.3 Converting the two-frequency system into a Hill equation. ....	37
4.4 Computational Algorithm: Step Function .....	39
4.5 Summary.....	43
<b>Chapter 5 Dynamic Stability Analysis and Vibration Responses.....</b>	<b>44</b>
5.1 Introduction .....	44
5.2 Dynamic instability regions of a pile.....	44
5.2.1 Dynamic instability from approximate Method (Harmonic Balance – (Hill-ID))..	45
5.2.2 Dynamic instability from Numerical Method (Step Function Method) .....	48
5.3 Calibration of the result from the Harmonic Balance Method .....	50
5.4 Quantitative solutions for vibration reactions .....	55
5.5 Impact of the Elastic Foundation.....	58

5.6 Impact of Damping ..... 61

5.7 Impact of dynamic and static component loads..... 64

5.8 Summary..... 67

**Chapter 6 Conclusions and Recommendations ..... 68**

6.1 Conclusions ..... 68

6.2 Recommendations for future research..... 70

**References ..... 71**

## Table of Figures

Figure 1.1 Soil-Pile Structure System .....	2
Figure 1.2 Soil-Pile Structure System .....	4
Figure 1.3 Types of Pile’s Failure .....	6
Figure 1.4 Elements of the seismic event on Treasure Island. ....	11
Figure 2.1 Pile foundation under axial load surrounded by soil .....	23
Figure 3.1 Instability Diagram - undamped .....	35
Figure 4.1 Parametric stimulation approximated behavior using step functions .....	40
Figure 5.1 Harmonic Balance Stability regions (Hill-ID regions) .....	47
Figure 5.2 Instability regions from the numerical simulation .....	50
Figure 5.3 The Mathematical Simulation's Instability Zones and the orders of Hill ID .....	51
Figure 5.4 Instability regions from the numerical simulation and 1-4 order Hill ID ....	52
Figure 5.5 Vibration response .....	56
Figure 5.6 Impact of dynamic load at different foundation rigidity levels: (a) $\eta = 0$ ; (b) $\eta = 0.5$ ; (c) $\eta = 1.0$ ; (d) $\eta = 2.0$ ; (e) $\eta = 3.0$ ; (f) $\eta = 4.0$ .....	58
Figure 5.7 Damping Impact: (a) $\delta = 0.1$ ; (b) $\delta = 0.2$ ; (c) $\delta = 0.3$ ; (b) $\delta = 0.4$ .....	62
Figure 5.8 The static component weight impact: (a) $\epsilon = 0.2$ ; (b) $\epsilon = 0.4$ ; (c) $\epsilon = 0.6$ ... .....	64
Figure 5.9 The dynamic element load impact: (a) $\lambda = 0.2$ ; (b) $\lambda = 0.4$ ; (c) $\lambda = 0.6$ ... .....	66

## Abbreviations

<b>Symbol</b>	<b>Description</b>
$A$	Cross-section area
$c_S$	Viscous damping coefficient
$D$	Flexural rigidity per unit width
$E$	Elastic modulus
$G$	Shear rigidity per unit width
$I$	Moment of inertia
$k$	Soil stiffness
$k_S$	Linear foundation stiffness
$L$	Length of pile
$L_e$	Effective length of pile
$M$	Moment
$n$	Mode number
$P$	Static axial load
$P(x, t)$	Subgrade reaction
$P(t)$	Dynamic axial load
$P_{cr}$	The critical Euler buckling load
$P_d$	Dynamic component of dynamic axial load
$P_n$	Euler load for $n^{\text{th}}$ mode of deformation
$P_S$	Static component of dynamic axial load
$q, q_n$	State function for the first mode of deformation ( $q_n$ for $n^{\text{th}}$ mode)
$T$	Period frequency of dynamic load
$t$	Time
$v$	Lateral displacement

<b>Symbol</b>	<b>Description</b>
$y$	Deflection
$\beta$	Damping coefficient
$\Gamma$	Gamma function
$\delta$	Logarithmic decrement of damping
$\delta(x)$	Dirac's delta function
$\epsilon$	Dimensionless dynamic load parameter
$\eta$	Dimensionless foundation stiffness parameter
$\theta$	Angular frequency of dynamic load
$\lambda$	Dimensionless static load parameter
$\rho$	Density
$\Phi(t)$	Axial loading periodic function
$\phi_i(x)$	Modal function
$\Omega, \Omega_n$	Natural frequency of a simply supported pile for the first mode ( $\Omega_n$ for $n$ th mode)
$\omega, \omega_n$	frequency of free vibrations of the pile loaded by force $P_s$ and constrained by soil foundation for the first mode ( $\omega_n$ for $n$ th mode)

# **Chapter 1 Introduction**

## **1.1 Introduction**

This chapter undertakes a comprehensive investigation into pile foundation engineering, encompassing foundational principles and advanced research in the field. The initial section systematically introduces the application and significance of pile foundations in megastructures and marine constructions. The discourse methodically progresses to encompass various types of pile foundations, emphasizing the imperative consideration of seismic excitation and analyzing the behavior of piles under such dynamic conditions. The chapter culminates by spotlighting pile failure behavior, with specific emphasis on the critical aspect of pile buckling.

In the second part, the academic focus shifts towards an in-depth exploration of research on pile foundation buckling instability. This scholarly inquiry extends to the importance of understanding dynamic stability in constructions subjected to multiple-frequency impulses. The chapter introduces the quasi-periodic Hill Equation and its related work, offering a sophisticated mathematical framework for addressing multiple frequencies. Concluding the academic exploration, the chapter delves into the modeling intricacies of building the basis using elastic pile modeling, setting the stage for subsequent academic endeavors in pile foundation design. This scholarly work serves as a foundational resource for academics, researchers, and practitioners seeking a comprehensive understanding of pile foundation design.

## **1.2 Pile's Purposes**

The special type of deep footing known as piles use combined surface friction and tip resistance to transmit weights from superstructures to the deeper levels of soil while supporting highly laden constructions. Additionally, they are used where the soil is delicate clay or scattered to fairly dense sand in seismically susceptible places (Rostami et al., 2020). They are widely used, especially when the building is to be placed on thin and weak layers of soil, in order to transmit tremendous weight from the superstructure into further down, robust levels of soil (Madabhushi et al., 2009).

### 1.2.1 A Synopsis of the Role of Pile

Their usage may be traced all the way back to ancient times if one so chooses. The Neolithic dwellers of Switzerland built their homes on logs they pushed into the soft foundations of small lakes around 12,000 years ago (Sowers, 1979). Venice was built on piles of timber in the swampy Po River delta in order to offer the first Italians shelter from attacks from Eastern Europe and to enable them to be nearer to the sea upon which their existence relied. Another case study is the Venezuelan Indians, who inhabited the lagoons surrounding Lake Maracaibo and resided in homes built on piles. For the purpose of building in locations with unfavorable conditions of soil for low-depth foundations, pile bases still have a place today (Prakash and Hari, 1991).

The pile-based foundation technique provides a reliable alternative for sustaining constructions in the situation of soft soil. As seen in the illustration that follows, Figure 1.1, this method allows the weight from the framework to be transferred to further down, tougher layers of soil. The elements of the piles may be required to endure thrusts when sustaining towering constructions that subject the base to prolonged periods of flipping. Whereas part of the weights are transmitted by shearing procedures that are formed along the shafts of the pile elements (shaft resistance), other sections are done so by typical strains that built up at their foundations (base resistance). They are referred to as end-bearing piles and drifting heaps, correspondingly (Jimenez, 2019).

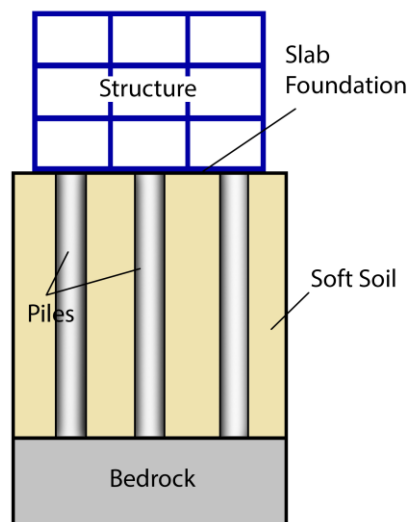


Figure 1.1 Soil-Pile Structure System (Jimenez, 2019).

## 1.2.2 Typical Functions of Piles

The most common usage of piles is to shift weights from shallower levels where their weight can't be adequately sustained to deeper levels where this is feasible. If a pile crosses through feeble substance and momentarily reaches another layer with strong bearing strength, the pile is said to be a bearing pile. If using piles in a deep layer with little sustaining capacity, frictional piles are employed because the piles get sturdier if placed close to each other. The combination of skin friction and point resistance frequently affects a pile's ability to support a weight. The rigid integration technique is furthermore considered as an interesting ground development method in weak soil conditions. This technique increases the ability of the ground to support buildings with simple weak foundations. The inflexible inclusion method and the pile foundation technique are equivalent, with the only difference being the inclusions' disconnection from the slab base. Nevertheless is important to note that these structures exhibit very distinct behaviors. In the solid inclusion structure, an LTP (Load Transfer Plant) sits amid the easily compressed layer and its outer structure. This reinforcing approach has a lot of benefits in seismic areas because the LTP acts as an energy dispersion area between the construction and the vertical rigid parts (Prakash and Hari, 1991).

## 1.3 A System of Classifying Piles

To narrow in on the many pile foundation categories, they might be divided into various classes based on how they function and sustain the weight:

- End-bearing piles: Employing the tip resistance provided by the piles, the framework's load is transferred from water or poorer soils to a robust load-bearing foundation (Figure 1.2a).
- Friction piles: The superstructure weight is transferred into the earth via the coefficient of friction created along the pile's axis (Figure 1.2b).
- Compaction piles, which are put into granular, porous soils to displace and compress the soil (Figure 1.2c).
- Tension piles are employed in both vertical and sloping configurations to sustain pull-out pressures. These piles are widely used for coastal constructions when the superstructure is expected to experience lateral stresses from earthquakes or gusts of

wind and the piles are used to hold tethers, cables, etc (Figures 1.2d and 1.2e) (Madabhushi et al., 2009).

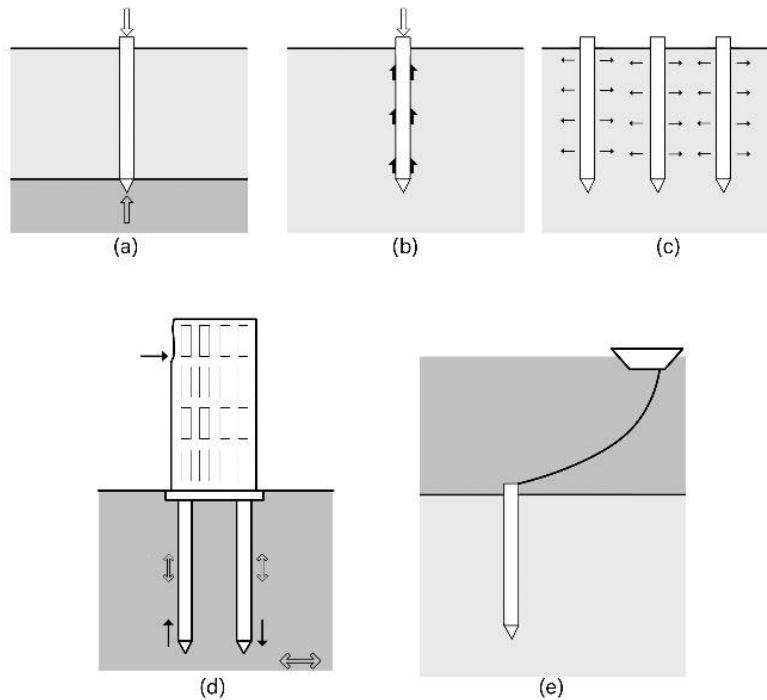


Figure 1.2 Soil-Pile Structure System. a) End Bearing Pile; b) Friction Pile; c) Compaction Pile; d) Onshore Tension Pile; e) Offshore Tension Pile (Madabhushi et al., 2009).

## 1.4 Pile Foundation Excited by Seismicity

### 1.4.1 Earthquake-Related Pile Behavior

When considering the manner in which a piled foundation responds throughout an earthquake, one must be aware of a few of the variables which could affect the piles' projected values. On laterally-loaded piles positioned in sandy soil, oscillations have been shown to have a considerable effect. When released while vibrating, piles reverted to their initial position. After a cycle of lateral pressure, vibration may probably help to reduce any residual bending in the pile. In machine bases, weights are placed on atop of the piles, which facilitates the estimate of machine instabilities. In clays, the loss of the pile's touch with the ground-level soil is more significant than vertical vibrations. Shear along the shaft of the pile is crucial in the torsional vibrations of a single pile, whereas the lateral stiffness of the pile and its position from the mass center of the pile group regulate the group stiffness and damping in a collection of piles.

Examining complex geotechnical issues requires an initial structure that describes a soil's behavior under varied loading circumstances. The critical state line is a line in the model where soils subjected to shear loads above a yield surface will try to cross before shearing can continue without changing the state of the soil (Stringer, 2012). In clays, the absence of soil contact by the pile at the ground's level is more significant than vertical vibrations. Shear along the longitudinal direction of the pile is crucial for torsional vibrations of a single pile, while group stiffness and damping in a set of piles are controlled by the lateral stiffness of the pile and its location from the mass core of the whole pile cluster.

Nonlinear loading during earthquakes will increase the operating loads of the piles. Identification of the seismic behavior of pile bases in liquefied soils is significantly more challenging owing to inconsistencies in the concepts fundamental to soil-pile-superstructure connection (which varies in forces, the rigidity and shear resilience of the soil in the vicinity, and the resulting production of pore water pressure). The seismic engineering of pile-supported structures has utilized a variety of planning methodologies in practice (Rostami et al., 2020).

For the soil pile structure, which may be conceived of as having an elastic component ( $\nu$ ), the modulus of shear ( $G$ ) and Poisson's proportion are important soil characteristics. The pile foundations may be excited by three separate oscillations: vertical tremors, linked horizontal sliding and swaying, and torsional tremors.

A soil element located in the sub-characteristic area will produce significant pressures in the pores throughout an earthquake, and the stress track will advance nearer to its origin up until it reaches the unique status line. When one reaches the line on one side of the  $p'$  axis, the strain's path ascends and descends like a wings of a butterfly passing past the point of origin or very near it. Pore stress and strain formation will also rise at this stage. If the applied deviator is sufficient to impact the usual state boundary on both ends, pore pressure will cycle at double the frequency of loading (Prakash and Hari, 1991).

When the enormous axial stress from the superstructure is applied, the pile would behave like an extended, laterally unsupported column and might budge, affecting the base in an earthquake. If the soil surrounding the pile loses a significant amount of its firmness and durability owing to liquefaction, this will occur during the whole tremors (Rostami et al., 2020).

### 1.4.2 Pile's Failure Types

The inertia of the foundation and/or kinetic pressures imposed on by lateral soil pressure are two possible reasons for pile collapse, as are axial load and bending. Dynamic breakdown (bending-buckling connection) of a base of piles may also occur in seismically liquefiable soil samples and result in the building collapsing (Figure 1.3). Potential pile types of failure include the ones listed below:

- 1) A differential in rigidity between liquefiable and non-liquefiable layers of soil that results in pile flexing or failure due to shear (Figure 1.3a).
- 2) A loss in load-bearing ability caused by liquefaction or stress relaxation in the soil combined with movement in the structures, resulting in tension pull-out, construction, or punching collapse in the piles (Figure 1.3b).
- 3) Pile collapse at the top is caused by substantial shifts and bending pressures at the point of contact with the cap or base slab, which often occurs with high constructions (Figure 1.3c) (Jimenez. 2019).

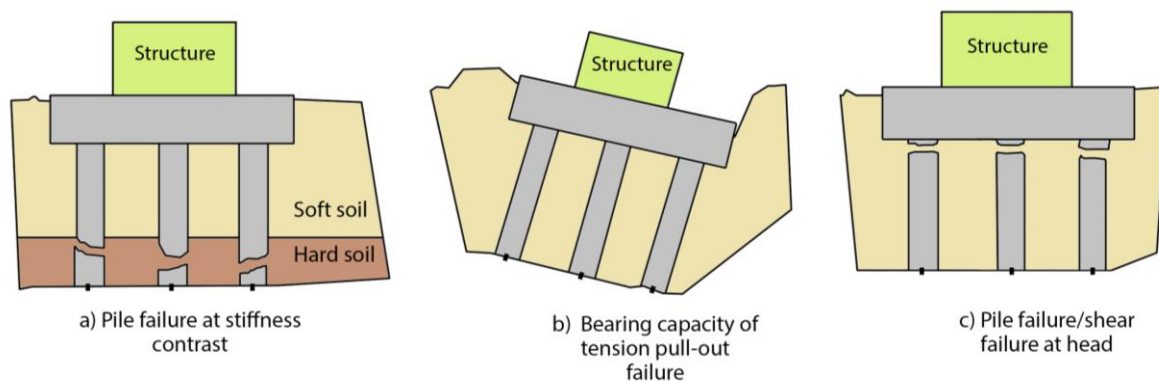


Figure 1.3 Types of Pile's Failure (Jimenez. 2019).

The bending failure process brought on by soil liquefaction-induced lateral expansion is often proven to be among the main causes of piling foundation failures throughout earthquakes. Bending failure, which results in the piles acting as fragile, unstable columns, may occur whenever soil liquefies and drops a considerable percentage of its rigidity. The strength of bending [for example, bending of the pile components] and flexural rigidity [changes in the shape of the moment-resisting pile segment] affect how a pile bends. In order to avert bend failure caused by lateral stresses when paired momentum and/or lateral distribution), the bulk of

modern design methodologies, such as JRA, NEHRP, IS:1893, and Eurocode 8, heavily emphasize the pile's flexibility (Rostami et al., 2020).

## 1.5 Research on Pile Foundation Buckling Instability

Several investigations on the issue of pile buckling have been done in the past few decades. Several of them were the subject of the present section of this research; they will be further addressed in terms of their predominance in the course of their publication:

The paper published by Yang and Ye in 2001 focused on the dynamic elastic local buckling of a perfectly geometrical pile subjected to an axial contact force. The importance of this computational investigation stems from the reality that buckling of an influenced bar under impact forces with temporary velocity often takes place after the wave of stress arrives at the tip of the bar, whereas instability frequently develops at the outset of the effect if it is exposed to a high-velocity impact force. The bulk of the pile and the impact of the stress waves' transmission along the pile's duration to the point where buckling occurs are both taken into account in this analysis. A perturbation technique is used to determine the crucial buckling length and the associated time frame (Yang and Ye, 2002).

The results showed that local dynamical elastic buckling occurred before the stress wave reached the pile ends. Although the elastic modulus, geometrical scale, and ratio of sub-grade reaction had significant effects on the unsteadiness, the impacts of skin friction and pile mass were minimal and could be ignored, according to the parametric evaluation resolved by differential equation (Yang and Ye, 2002).

In comparison to the Winkler model with the Euler beam, the suggested model greatly outperforms it in terms of the dynamic interaction of piles positioned in stiff soil with low slenderness ratios. The relationship between variables generated by the current model may be simply applied to the investigation of the changing reaction of pile sets by making use of the superposition idea. The existing double-shear model could be extended to take into consideration the interaction of piles in the soil if the rigidity variables and damping ratio of the saturated substrate were given (Wang et al., 2014).

Lee's study from 2018 presents a general model that continues to evaluate the flexural behavior and buckling of partially immersed end-bearing piles that experience axial compressive

force. The Runge-Kutta approach and the Regula-Flasi approach are methods that are suggested for analyzing the differential equation that governs the motions. The recommended model's accuracy is confirmed through the comparison of the observed findings with the most recent numerical solutions, which, in terms of engineering, permits the creation of the optimal soil system layout. The results demonstrate that distinct changes in administered compressive force have a significant impact on how the behavior of the soil-pile complex behaves in relation to its intrinsic frequency. As the axial compressive force reaches the buckling load, the unrestrained vibration impact on the structure stops contributing, signaling the buckling (Lee, 2018). In 2020, two other studies were carried out in a similar way:

First is an article published by Liu, et al (2020) constructed an analytical framework to determine the equilibrium equations and boundaries. The boundary value problem was subsequently computationally resolved using Matlab software to ascertain the crucial load for buckling and buckling form. The buckling behaviors of a curved friction pile submerged in mixed soil are carefully examined through taking into consideration both the linear shaft friction and linear lateral rigidity of the soft soil because buckling fluctuation of thin, lengthy piles in soft soils is an essential consideration in geoenvironment layout. The results show that the buckling load is significantly influenced by the friction ratio and that the buckling load increases as the friction ratio lowers. The maximum dimensionless buckling strain in the curved friction pile with linear shaft friction has an optimal tapered ratio as well (Liu et al., 2020).

Determining if a functionally graded beam with a Terfenol-D covering may be employed as a vibration dampening component for a rocket sledge system was another goal of Patil and Kadoli's investigation from the same year. This research adds to a series of works that examine the use of the Terfenol-D layer with the metal-ceramic functionally graded beam. Terfenol-D is a smart material with a high-power density, broad bandwidth, strong force, and enormous strain as its inherent properties. Under the influence of linear momentum, shock, trembling, acceleration, and aerodynamic impacts, the researchers employ the rocket sledge technique. The researchers have constructed the theoretical framework for a dynamically graded Terfenol-D composite beam standing on a Winkler-two factor elastic basis and a viscoelastic foundation relying on the Euler-Bernoulli beam concept. The answer to the next equation yields the two collections of eigenvalues. The slightest one is consistent with the longitudinal movement of the FGMT beams (Patil and Kadoli, 2020).

Yet, as of 2022, the most current of these studies are outlined below:

There aren't currently any studies on the evaluation of the dynamic stability of pile sets under stress wave, according to Yao and Shi's research. This subject is important given that recently, as marine assets have been utilized, there has been a huge increase in the amount of offshore constructions. The majority of these structures is pile and pile group bases. It is more challenging to manage the relationship between heaps in a set of piles than it is with an individual pile. The principle of diffraction, the modified Vlasov foundation model, and the concept of dynamics are all used by investigators in the development of the high-order vibration differential equation. For the purpose of analyzing pile group settlement, the Poulos approach is used. The authors use the relationship component methodology and transfer matrix approach to create the dynamic equilibrium equations for the active pile and passive pile. Findings show that, for pile groups, displacement develops linearly with increasing wave height  $H$  and nonlinearly with increasing wavelength  $L$  (both variations being significantly lower than those of the single pile) (Yao and Shi, 2022).

Gu, et al, along with others completed one more of the aforementioned investigations in which they showed that pile foundations are widely used to provide reinforcement for offshore constructions. The study shows that wave pressures and ship collisions can cause a pile-soil system to become unstable or fail. To assess the dynamic stability of piling foundations for offshore structures, they employ wave loads and SIs. The two-parameter foundation model and Galerkin integral technique have been used to generate the nonlinear dynamic differential control formulae for offshore structures. Likewise, the pile body's dislocation function and instability load are calculated using the fourth-order Runge-Kutta technique and the shift time-history curve, respectively (Gu et al., 2022).

Lastly, Shan et al. (2022) concentrated on several shortcomings in earlier studies on floating piles. As of right now, the two primary modes are the Winkler model and the overlay virtual rod model. The spring rigidity and damping factor of the Winkler model, on the other hand, were mainly calculated by tests and do not correspond to normal soil dynamic parameters. The impact of the pile end soil thickness and specific attributes on the behavior of vibration cannot be taken into thought in this model simply because of the difficulty of accounting for the unsaturated nature of soils. On top of that, nothing is known about the soil's three-phase medium. In light of

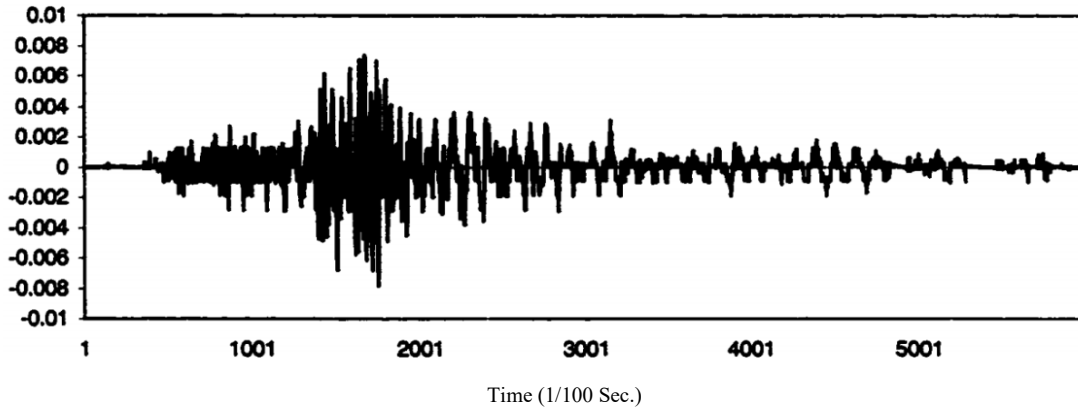
this, the researchers provide in their study a sophisticated analytical approach to the vertical behavior of a floating pile in homogeneous unsaturated soils (Shan et al., 2022).

## **1.6 Dynamic stability of constructions undergoing quasi-periodic frequency**

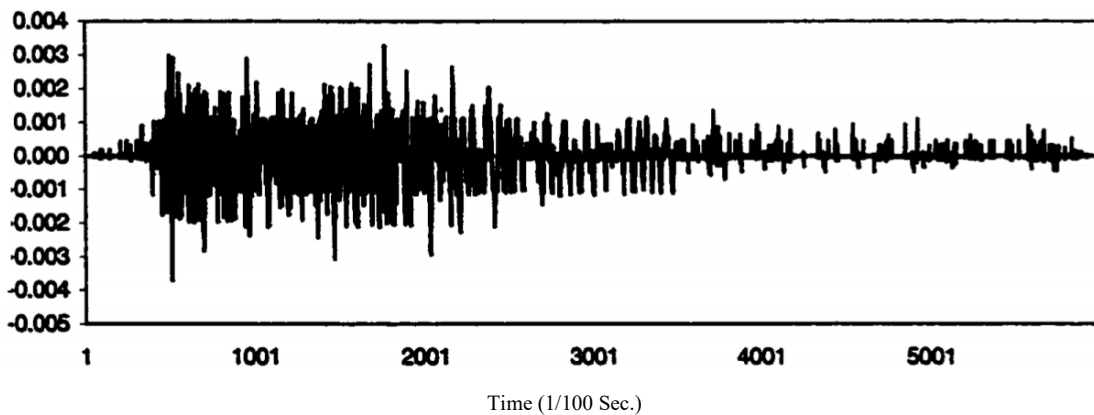
### **1.6.1 The objective of employing Quasi-Periodic Waves in Structural Design to Model Seismic Dynamic Loads**

In the realm of professional academic studies, the investigation of seismic events takes center stage due to the significant real-world impact of earthquakes, marked by high Richter magnitudes resulting in widespread destruction, financial implications, and loss of life. The pivotal consideration lies in designing structures resilient to seismic waves, particularly in regions prone to such geological activities. Two fundamental parameters influencing the behavior of seismic waves are the magnitude of the dynamic load and the frequency of the wave. Traditional studies have often assumed seismic waves to be periodic, but the actual earthquake excitation, as visually demonstrated, defies periodicity. This deviation from periodic behavior necessitates a more nuanced approach to modeling seismic waves to capture their true nature. To address this, the study advocates for the utilization of quasi-periodic frequencies as a more accurate representation of the non-periodic nature of earthquake excitations. This approach challenges the conventional assumption and offers a more realistic perspective in understanding seismic phenomena. (Liu, 2001; Plaut et al., 1986; Plaut and Hsieh, 1985).

Ground acceleration records, vital for this research, are obtained from various online repositories, with a particular emphasis on excitation data. A notable illustration is the ground motion record presented in Figure 1.4, stemming from the Treasure Island earthquake that occurred on September 3, 2000. Figure 1.4 visually presents the ground motion record, encompassing both horizontal and vertical components. The accessibility of each record at 0.01-second intervals, amounting to a minute-long record, provides a wealth of data for in-depth analysis. This methodology not only contributes to a more comprehensive understanding of seismic waves but also enhances the potential for designing structures capable of withstanding the dynamic challenges posed by real-world seismic events (Liu, 2001).



(a) Horizontal component



(b) Vertical component

Figure 1.4 Elements of the seismic event on Treasure Island. (Liu, 2001)

Moreover, incorporating quasi-periodic frequencies into seismic wave modeling aligns with the cutting-edge advancements in seismic studies. It reflects an interdisciplinary approach, drawing on insights from geophysics, structural engineering, and data science. The integration of diverse knowledge domains facilitates a holistic exploration of seismic dynamics, enriching the academic discourse and advancing the practical applications of seismic research. In conclusion, this professional academic study not only highlights the pressing need for resilient structural design in seismic regions but also advocates for a paradigm shift in modeling seismic waves through the incorporation of quasi-periodic frequencies. The utilization of real-world seismic data and the exploration of non-periodic characteristics contribute to a more accurate representation of seismic events, fostering advancements in seismic research and applications (Liu, 2001; Plaut et al., 1986; Plaut and Hsieh, 1985).

## 1.6.2 Study on Quasi-Periodic and Its Application Rationale

Linear ordinary differential equations with time-periodic factors are used in a wide variety of scientific and engineering fields. Examples include periodic load-bearing structures, helicopter rotor blades that fly forward, unbalanced rotor-carrying systems, monotonous job robots, ship dynamics, satellite attitude balancing, heartbeats, and quantum physics. These systems are sometimes referred to as "parametrically stimulated systems" since the system properties in computational models are no longer static but have changed into periodic functions of time. "Parametric resonance" is a situation that may result from these functions. In order to anticipate the stability and behaviour of linear ordinary differential equations with recurring parameters, M.G. Floquet developed a thorough theory in 1883. The "Floquet Theory" is the name given to this hypothesis. Since then, several computational, mathematical, and symbolic methods for determining the stability and responsiveness of periodic systems have made use of this notion. Some authors used piecewise constant, linear, and quadratic matrices (functions) to approximate the periodic coefficient matrix (periodic functions). Friedmann et al. created a quantitatively efficient method that only requires one integrator pass scheme by combining Hsu's approach with Hammond's increased coupling method. A few papers have evaluated the stability of periodic systems using analytical techniques like perturbation and norm aging. However, its usefulness is constrained by the requirement for an insignificant variable and producing results. To overcome the aforementioned limitations, Sinha and his colleagues developed an efficient approach for computing the transition state matrix (STM) of such systems in semi-analytical as well as figurative formats. The development of control systems that compel chaotic, erratic movements into periodic orbits also uses the Floquet theory (Sharma and Sinha, 2018).

The academic literature contains a wealth of contributions pertaining to usage. Mathieu or Hill equations have traditionally been employed to model systems because Floquet theory may be utilized to forecast a system's stability and responsiveness. However, in many cases, they are oversimplified models since the parametric stimulation is quasi-periodic rather than cyclic because it consists of inconsistent frequencies. Parametric stimulation occurs, for instance, when a ship is moving in the course of the waves or when the sea waves are passing over the whole breadth of the ship. When the vertical pull brought on by the sea waves is taken into account as a periodic force, the formula for the equation of motion is determined to be a Mathieu/Hill equation. On the other hand, sea waves have discordant frequencies and are not by definition

periodic. The motion of a heart and the basilar membrane (BM) in the cochlea of the inner ear are two other examples where the parametric driving terms would not be thought of as periodic. A proper cardiac model can be used to identify any abnormalities or illnesses. The BM fluctuations of the cochlea of the inner ear have been unknown for a long time. Following this, several researchers established that BM receives parametric stimulation and that dynamic computing using the Floquet theory may be done in the context of single-tone (frequency) inputs. Considering the structure of sound (speech signal) is often complex, two or three-tone motions must first be investigated in order to understand what happens under complex stimulus. Deformation consequences (mixtures of tones) were discovered by Robles et al. and Ruggero et al. in their investigations of the brain's response to two-tone stimulation. The genesis of quasi-periodic motion may alternatively be explained by the first Hopf bifurcation (also known as the Neimark-Sacker bifurcation) of a fixed position, which yields a periodic response (limit cycle). A periodic motion or a quasi-periodic motion may occur from this secondary Hopf bifurcation. When attempting to investigate the stability of the associated quasi-periodic motion, one must first construct the variational equation pertaining to this motion. (Sharma and Sinha, 2018).

The control of instabilities in such structures is just as important as determining which sections are stable or unstable. To create an efficient control system, one must take into account the quasi-periodic behavior of these parametrically stimulated systems. Control tools are also used during heart surgery to reduce the motion of a beating heart component over which the operation must be performed. Even though all of these problems require a conceptual framework to describe how they behave and govern, there isn't a full framework for linear differential equations with quasi-periodic coefficients (Sharma and Sinha, 2018).

### **1.6.3 Research on dual-frequency excitation in the realm of civil engineering**

Research into dual-frequency excitation within the field of civil engineering has been undertaken. Presented below are instances of some of the more recent studies.

Sahoo et al. (2016) investigated the intricate nonlinear dynamics of an axially moving viscoelastic beam when subjected to dual-frequency parametric stimulation, with an emphasis on the interaction of combination resonances between the first two modes under a 3:1 internal resonance scenario. By applying the direct method of multiple scales, the complex nonlinear integral-partial differential equation that controls the beam's lateral movement is simplified,

unveiling behaviors such as stability, quasi-periodicity, and chaos, which vary according to the system's parameters, including frequency detuning and pulsation amplitude. The numerical analyses underscore the depth of nonlinear phenomena not previously discussed in the literature on axially moving systems, presenting findings with tangible benefits for the design and analytical assessment of these structures. Through exhaustive parametric research, this study reveals previously unidentified zones of instability, a range of bifurcations, and a variety of dynamic actions, thereby greatly enriching the comprehension of nonlinear dynamics in axially moving viscoelastic beams exposed to complex stimulations (Sahoo et al., 2016).

Zhao et al., 2018 is delved into by exploring how fluctuations in temperature are affected on the nonlinear vibrational responses of hanging cables when exposed to dual-frequency stimulations, with both combined and concurrent resonance effects being particularly highlighted. A mathematical formulation that incorporates the impact of thermal variations on cable tension is introduced, with the Galerkin technique being utilized for the discretization of nonlinear dynamic equations. Through perturbation analyses and stability assessments being conducted, it is indicated that shifts in temperature are found to considerably alter both the qualitative and quantitative dynamics of cable vibrations, which are influenced by the sag-to-span ratio and the extent of temperature change. Computational findings illustrate how the vibrational attributes of cables, such as resonance amplitude and phase, are significantly impacted by temperature, being intricately linked to the sag-to-span ratio. The intricate relationship between thermal fluctuations, nonlinear vibrational characteristics, and the structural parameters of hanging cables is underscored by this investigation, with valuable perspectives for their design and evaluation in diverse environmental scenarios being provided (Zhao et al., 2018).

Cong et al., 2021 have been investigated the complex dynamics exhibited by cable-stayed cantilever beams, which are subjected to dual-frequency stimulations, and delve into various types of resonances such as primary, sub-harmonic, and super-harmonic. The Galerkin technique, along with a multiscale approach, is employed, demonstrating how crucial roles are played by fluctuations in temperature in influencing the vibrational behavior of these structures, thereby underscoring the profound links that are found between climatic changes and structural dynamics. How varied responses are elicited from the cable and beam by different types of excitations is further exposed by the research, noting how significant effects are had by the

amplitude and frequency of excitations on the system's stability and vibrational patterns. Through detailed parametric analyses that are conducted, the intricate dynamics of cable-stayed structures under complex excitations are showcased, with crucial insights being offered for their design and analytical evaluation towards improving structural robustness (Cong et al., 2021).

The research has been investigated by Zhang et al., (2021) delves into the dynamic equilibrium of viscoelastic beams that are axially transported, subject to parametric excitation at two frequencies alongside a 1:3 internal resonance. By employing the direct method of multiple scales, the study examines the repercussions of such stimulations and resonance on the system's stability frontiers. Noteworthy discoveries encompass the detection of irregular and multiple-valued stability frontiers, underscoring the profound influence of dual-frequency stimulation and internal resonance on the stability of the system. The research showcases that an enhancement in the coefficients of viscoelasticity can diminish zones of instability, and it stresses the necessity of accounting for non-uniform boundary conditions to prevent an overestimation of system stability. Confirmations through numerical methods, specifically the differential quadrature method, affirm the theoretical findings, highlighting the intricacies and susceptibilities of axially transported viscoelastic beams to such parametric excitations and internal resonances (Zhang et al., 2021).

The research has been investigated by Zhang et al. (2022) delves into the nonlinear behavior of viscoelastic beams in axial motion, subjected to excitation at two frequencies, with a particular focus on 3:1 internal resonance. Employing the Kelvin-Voigt model for viscoelasticity characterization, a mathematical structure is established to examine how the beam's vibrational characteristics are influenced by material attributes and external excitations. Through both analytical and numerical investigations, which utilize the method of multiple scales for deriving approximate solutions and the differential quadrature method for empirical confirmation, the study uncovers various complex vibrational phenomena. These include interactions across multiple modes, alterations in stability, and the emergence of bifurcation patterns. The results highlight how the dynamics of the system are significantly impacted by the coefficients of viscoelasticity, illustrating that an increase in these coefficients can promote system stability through the dissipation of vibrational energy. By offering new insights into the complex vibrations of axially moving viscoelastic beams, this research makes a valuable contribution to

the field, providing knowledge that is crucial for the design and management of such systems within engineering contexts (Zhang et al., 2022).

## 1.7 Quasi-Periodic Hill Equation and Related Work

A modified damped Mathieu/Hill equation with the following solution can be used to represent one of the most basic types of linear differential equations with quasi-periodic coefficients.

$$\ddot{x} + d\dot{x} + (a + b_1 \cos \omega_1 t + b_2 \cos \omega_2 t)x = 0. \quad (1.1)$$

where  $a, b_1, b_2$  and  $d$  are system parameters;  $t$  is the time; and  $\omega_1$  and  $\omega_2$  are the two parametric frequencies (Sharma and Sinha, 2018).

Numerous authors have looked into the stability of this kind of system in the past. Using the multiple scale technique, Davis and Rosenblat investigated the QP Hill equation and calculated the stability boundaries in 1980 (Davis and Rosenblat, 1980).

They claim that stability boundaries for both types of families,  $a = (k_1 \omega_1)^2/4$  and  $a = (k_2 \omega_2)^2/4$ , originate from an axis where  $k_1, k_2 = 0, 1, 2, \dots$ . The relationship between the rotation number ( $\alpha$ ) of a nearly periodic function and the frequency component ( $M$ ) in the spectral gaps was demonstrated by Johnson and Moser,  $2\alpha \in M$  (Johnson and Moser, 1982).

The whole parametric field is consistent with this relationship. Rotation number has been employed by various researchers to depict the stability diagrams since it is independent of the specific solution and equals  $\sqrt{a}$  when  $b_1 = b_2 = 0$ . Using the findings of Johnson and Moser (Johnson and Moser, 1982) as a starting point, Zounes and Rand explored the QP Hill equation computationally (Zounes and Rand, 1998).

First, the Lyapunov parameters were calculated and straight computation was used to create the stability diagrams. An excellent fit between analytical and computational results was observed later in their study when formulas for transition curves were generated using normal perturbation and an approach resembling Hill's method of infinite determinants.

These authors claimed that zones of instability in the  $a \sim b$  plane come from the axis at  $a = (k_1 \omega_1 \pm k_2 \omega_2)^2/4$ ;  $k_1, k_2 = 0, 1, 2, \dots$  where the primary areas of instability are caused by the expressions  $a = \omega_1^2/4$  ( $k_1 = 1, k_2 = 0$ ) and  $a = \omega_2^2/4$  ( $k_1 = 0, k_2 = 1$ ).

Additionally, they claimed that the damping has a greater impact on the higher-order resonances contrasted with the lower-order resonances. The QP Hill equation was statistically investigated by Broer and Simo (1998) with two parametric frequencies:  $\omega_1 = 1$  and  $\omega_2 = (\sqrt{5} + 1)/2$ . Using the maximum Lyapunov exponent and rotation number, they numerically tested the stability boundaries for rather large parameter values (in comparison to Zounes and Rand, 1998). In 2011, Puig and Simo looked into the stability bounds in a QP Hill's equation with three parametric ( $\omega_1 = 1, \omega_2 = \sqrt{2}$  and  $\omega_3 = \sqrt{3}$ ) and they plotted the bounds employing rotation number and maximal Lyapunov coefficient (Puig and Simó, 2011).

While the implementation of Hill's infinite determinants technique to the QP Hill equation grows increasingly laborious with systems of greater complexity and with a greater number of terms in the generalized Fourier series, perturbation and averaging strategies demand a number of minor variables and providing solutions. The infinite determinants of the Hill are recognized to not merge in all circumstances (Broer and Simó, 1998; Davis and Rosenblat, 1980; Johnson and Moser, 1982; Puig and Simó, 2011; Sharma and Sinha, 2018; Waters, 2010; Zounes and Rand, 1998). Lyapunov coefficients and rotation numbers can be used to create stability graphs, however, this requires a lot of computing resources and fails to offer you any statistical data.

Deng (2023b) introduced a novel numerical method for analyzing the stability of columns under dynamic loads with multiple frequencies. The equation of motion for columns with fixed-fixed connections under parametric loads was derived and decoupled into an ordinary differential equation with variable coefficients representing multiple frequencies. The first step of the numerical method involves approximating the system with multiple frequencies by an equivalent system with a single frequency (or period  $T$ ) as closely as possible. Subsequently, the period  $T$  is divided into a sufficient number of equal time intervals. On each interval, the system is approximated by an equation of motion with constant coefficients, which can be readily solved. The responses on each interval within one period  $T$  are accumulated. Stability analysis can then be conducted using the state transition matrix.

## 1.8 Building the Basis with an Elastic Pile Modelling

The type of foundation significantly influences how a beam interacts with it. Several articles have provided a detailed analysis of the interaction between a beam and a foundation. During the

nineteenth century, beams on elastic bases were initially used for examining railway tracks. (Ahuja and Duffield, 1975; Gabr et al., 1997; Iwatsubo et al., 1973; Shahroudi, 2023; Tanahashi and Suzuki, 2020; Yokoyama, 1988)

Following, several other mechanical representations have been proposed for studying stable soil-structure relations. The mechanical systems of soil were summarized, and their uses were discussed by Tanahashi (Tanahashi and Suzuki, 2020). Table 1.1 provides the controlling formula and design graphic for every mechanical model.

Table 1.1 Models for mechanical soil (Liu et al., 2020).

Soil's Model		Deflection Curve of the Surface
Model with one parameter	Winkler	<p><math>k</math>: Coefficient of subgrade reaction</p>
Model with two parameters	Filonenko - Borodich	<p><math>k</math>: Coefficient of subgrade reaction <math>T</math>: Tensile member</p>
	Hetenyi	<p><math>k</math>: Coefficient of subgrade reaction <math>D</math>: Flexural rigidity</p>
	Pasternak	<p><math>k</math>: Coefficient of subgrade reaction <math>G</math>: Shear rigidity</p>

The source is the juncture at which the soil is loaded, whereas  $x$  stands for distance and  $y$  for deflection. They fall into one-parameter designs and two-parameter model categories based on their parameters.

According to the Winkler method, which is the most basic possible one-parameter model for perpetual systems (Engel, 1991), an ongoing system is made up of distinct, isolated longitudinal springs whose response forces are equivalent to their shifts. Further examples are the Pasternak Model (with shear component), Hetenyi Model (with torsional element), and Filonenko-Borodich Model (with tensile element) (Tanahashi and Suzuki, 2020). These include a component over the springs in an effort to remedy the Winkler Model's interruption flaw.

Mastering these sorts of bases' static performance is crucial when trying to comprehend their dynamic activity. Additionally, it is essential to investigate how the outside environment affects dynamic equilibrium in order to comprehend how these substances will respond to various kinds of time-dependent pressures.

Sugiyama stated that it is feasible to estimate an ongoing structure with a distinct system (Iwatsubo et al., 1973). Ahuja investigated the measured reaction of a beam with a varying cross-section that was supported by an elastic base and exposed to the dynamic axial stress condition using combined empirical and theoretical methods (Ahuja and Duffield, 1975). Using the Winkler-type basis, he claimed that both theoretical and empirical results reveal the precise bounds of the unstable zone. Employing finite element techniques, Yokoyama examined the behavior of a Timoshenko beam supported by an elastic base modeled by Winkler in 1987 (Yokoyama, 1988). The natural rates, stable buckling weights, and dynamic oscillations induced by elastic bases of Timoshenko beams with various endpoint circumstances were examined. In 1997, created a model to assess the essential buckling performance of long, thin piles of friction with horizontal foundation soil based on the subgrade response concept. The measurement value of the subgrade response ( $k_h$ ) is calculated within the model using a generic power distribution. The integrity of a thin pile with various tip and top stabilizers (pinned, set, or loose termination) was the subject of the investigation (Gabr et al., 1997).

A beam supported by viscoelastic bracing was employed by Engel (1991). Engel has included the fluid damping of the bearing substance into the Winkler, Hetenyi, and Pasternak basis models. He identified the unstable zones and the crucial dynamic forces using the Floquet

concept. He provided an example of how the basis's characteristics of viscous damping affected its rigidity behavior. Additionally, he contrasted the instability limit under the various buckling displacement types and the results of the various soil pile interface theories.

## 1.9 Thesis Outline

The preceding thesis commenced in Chapter 1 with an exploration of pivotal considerations in pile foundation design, highlighting their critical role in megastructures and marine construction. The two-part investigation covered fundamental aspects of pile foundations, seismic influences, and pile behavior, with a specific focus on buckling. The second part delved into sophisticated research on pile foundation buckling instability, emphasizing dynamic stability and introducing the Quasi-Periodic Hill Equation. The opening chapter underscored the imperative need to comprehend these aspects as a foundational requirement for subsequent chapters on pile foundation design.

Moving forward, the second chapter will be dedicated to intricately modeling pile foundations under dynamic loads, encompassing both single and dual frequencies. The central focus will involve constructing a beam model supported by a Winkler foundation, incorporating a pair of frequencies. The derivation of the equation of motion will utilize equilibrium formulas and transform a partial differential equation into an ordinary one through the Galerkin technique. This chapter will set the stage for subsequent discussions by presenting the fundamental equation that will be refined in later chapters.

The third chapter will shift the exploration towards the investigation of the stability diagram of a pile foundation under dual-frequency dynamic loading. Utilizing the Harmonic Balance technique, the chapter will employ Hill's infinite variables to formulate transition curves, revealing instabilities within the V-shaped region. This chapter will stand as a substantial contribution to understanding pile foundation dynamics and the phenomena of instability under dual-frequency excitations.

Chapter four will build upon the step function method as a numerical method for investigating stability diagrams with dual frequency. It will first convert a two-frequency system into a Hill equation with a single primary frequency. The chapter will introduce a computational

algorithm using step functions for the undamped Mathieu-Hill equation, providing insights into dynamic stability.

The fifth chapter will provide an in-depth exploration of dynamic instability regions in pile foundations by offering a case study, with a focus on seismic events. Utilizing the Harmonic Balance method and the numerical Step Function method, the chapter will systematically analyze stability diagrams under dual-frequency excitations. It will emphasize the accuracy of the computational modeling, showcasing insights into the dynamic behavior of pile foundations under various conditions.

In conclusion, Chapter 6 marks the culmination of this research endeavor, summarizing the exploration into dynamic stability and vibration reactions of piles on elastic bases subjected to oscillating axial forces. The proposed computational algorithm's precision and reliability, compared to the traditional Harmonic Balance method, are emphasized. The chapter focuses on calibrating rough instability limits using Hill infinite factors, addressing their accuracy and limitations. Vibration reactions are analyzed, validating computational instability charts and comparing results with the fourth-order Runge-Kutta method. The study's significance in mechanical and civil engineering is underscored, hinting at potential future research directions.

## **1.10 Summary**

This chapter elucidates the critical considerations in pile foundation design, emphasizing their importance in megastructures and marine construction. Divided into two parts, the first part covers the basics of pile foundations, seismic influences, and pile behavior, particularly focusing on buckling. The second part delves into advanced research on pile foundation buckling instability, emphasizing dynamic stability, and introducing the Quasi-Periodic Hill Equation. The chapter underscores the significance of understanding these aspects as a prerequisite for subsequent chapters on pile foundation design.

## Chapter 2 A Model of Pile Foundations Under Seismic Excitations

### 2.1 Introduction

This chapter will delve into the modeling of pile foundations under dynamic excitation, considering both single and dual frequencies. The aim is to systematically analyze the structural response of pile foundations in these dynamic scenarios, providing valuable insights and contributing to the scholarly understanding of pile foundation dynamics.

### 2.2 Problem formulation

In order to study buckling unsteadiness, piles encased in soil adjacent to them can be thought of as beams supported by alternatively a flexible or a viscoelastic basis. The fixed flexure and dynamic responses of these beams, which are supported by various elastic and viscoelastic bases, have drawn the attention of many investigators. Many scholars choose the Winkler model in their dynamic studies notwithstanding it showing an absence between loaded and unloaded modes because of its simple method for solving problems (Engel, 1991). The Winkler model is used in the present research to illustrate the soil circumstances encircling the pile foundation.

We evaluate a tiny vertical section in a pile and create a motion formula for that specific section to test the sturdiness of the pile. The unique qualities of the vertical piece and the surrounding substance are taken into consideration when creating this formula. For this specific inquiry, we will use the force equilibrium technique. Usually, the motion equation is derived from one of the force balance or energy equilibrium formulas.

A pile with a stable cross-sectional form, a length of  $L$ , and  $EI$  as its flexural stiffness is shown in Figure 2.1 which is a first-order approximation. The pile is restricted by the nearby earth composition to prevent lateral deformation while receiving straightforward assistance at its dismissals and maintaining a pin-pin shape.  $p(x, t)$  represents the subgrade response for every pile length in the setting of Figure 2.1, taking into account the effects of springs and dampers. Furthermore, the force ( $ma$ ) is equivalent to the energy force (D'Alembert's force), which opposes particle dislocation and is denoted by the symbol ( $\rho A \Delta x \ddot{v}$ ). In this formula,  $A$  stands for the cross-sectional area and  $\rho$  stands for the mass concentration of the pile per unit capacity.

Given the dynamic axial stress,  $v$  additionally describes an estimate that depends on both  $x$  and  $t$ .

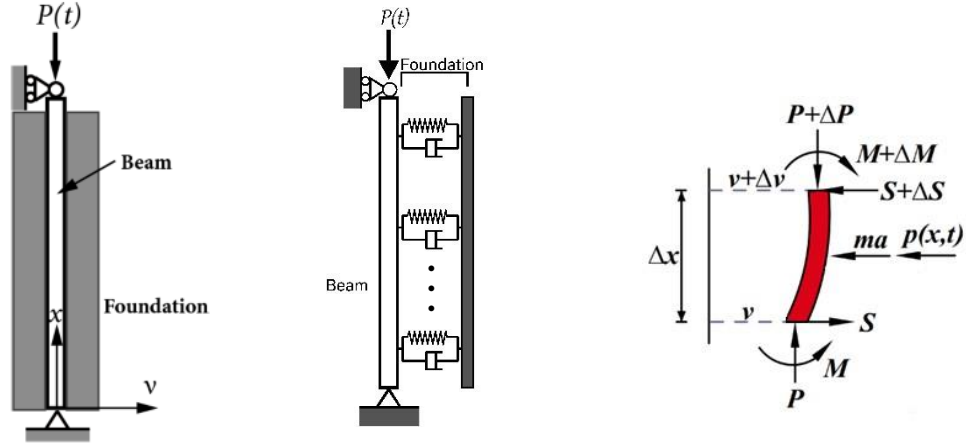


Figure 2.1 Pile foundation under axial load surrounded by soil. (Engel, 1991; Deng et al., 2023)

Consider the formulae for the micro pile segment's balance. It is presumed that  $\Delta P = 0$  when adding the loads across the vertical line  $x$ . The subsequent formula is produced by averaging the loads horizontally in vector  $v$ .

$$(S + \Delta S) + (\rho A \Delta x) \ddot{v} - S + p(x, t) \times \Delta x = 0 \Rightarrow \frac{\Delta S}{\Delta x} = -\rho A \ddot{v} - p(x, t). \quad (2.1)$$

Bringing together the instant at the pile segment's halfway results in:

$$\begin{aligned} (M + \Delta M) + P(t) \times [(v + \Delta v) - v] - M - (S + \Delta S) \times \Delta x - (\rho A \Delta x) \ddot{v} \times \frac{\Delta x}{2} - p(x, t) \Delta x \times \frac{\Delta x}{2} &= 0. \\ \Rightarrow \Delta M + P(t) \times \Delta v - (S + \Delta S) \times \Delta x - (\rho A \Delta x) \ddot{v} \times \frac{\Delta x}{2} - p(x, t) \Delta x \times \frac{\Delta x}{2} &= 0. \end{aligned} \quad (2.2)$$

$$\frac{\Delta M}{\Delta x} + P(t) \times \frac{\Delta v}{\Delta x} = (S + \Delta S) - \frac{\Delta S}{2}. \quad (2.3)$$

The formulas of Equation (2.1) within Equation (2.3) are altered to have the limit of  $\Delta x$  approaches zero.

$$\frac{\partial S}{\partial x} = -\rho A \ddot{v} - p(x, t), \text{ and} \quad (2.4)$$

$$\frac{\partial M}{\partial x} + P(t) \times \frac{\partial v}{\partial x} = S. \quad (2.5)$$

After concluding Equation (2.5) with regard to  $x$ , we get:

$$\frac{\partial^2 M}{\partial x^2} = \frac{\partial S}{\partial x} - P(t) \times \frac{\partial^2 v}{\partial x^2}. \quad (2.6)$$

In Equation (2.6), replacing (2.4) results in:

$$\frac{\partial^2 M}{\partial x^2} = -\rho A \ddot{v} - p(x, t) - P(t) \times \frac{\partial^2 v}{\partial x^2}. \quad (2.7)$$

On the other hand, with a flexible beam, the connection between Moment and Curvature (Xie, 2006) is:

$$M = EI \frac{\partial^2 v}{\partial x^2}. \quad (2.8)$$

The formula for the rate of velocity for the pile can be written by substituting Equation (2.8) for Equation (2.7). This equation only valid for constant E and I.

$$EI \frac{\partial^4 v}{\partial x^4} + P(t) \frac{\partial^2 v}{\partial x^2} + \rho A \frac{\partial^2 v}{\partial t^2} + p(x, t) = 0. \quad (2.9)$$

Piles are usually subjected to variable axial stresses in addition to static axial loads. Dynamic loads can take a variety of shapes, including earthquakes, vibrations from mechanical components, and engineering explosives (Shahroudi, 2023; Deng et al., 2019).

The soil's responsive pressure throughout the length of the pile is determined through taking into consideration the damping impact within the soil around the pile.

$$p(x, t) = k_s v + c_s \frac{dv}{dt}. \quad (2.10)$$

In this instance,  $k_s$  stands for the longitudinal foundation's rigidity, and  $c_s$  stands for the soil foundation's dampening viscous ratio. Furthermore,  $c_s v$  represents the soil-derived damping force. Borrowing from Equation (2.10) and Figure 2.1, it can be seen that the soil on the opposite end of the pile causes the pulling force of springs to be transferred to the left while the pile deflects to the right (in the positive  $v$  orientation). In contrast, the spring force is directed to the right once the pile rotates to the left (in the negative  $v$  orientation) because of the soil on the pile's left edge. The mechanics of soil modeling takes into account the integrated response of the soil medium on each side of the pile, as shown in Figure 2.1.

Formula (2.10) is changed into Equation (2.9), and the result is:

$$EI \frac{\partial^4 v}{\partial x^4} + P(t) \frac{\partial^2 v}{\partial x^2} + \rho A \frac{\partial^2 v}{\partial t^2} + \left( k_s v + c_s \frac{dv}{dt} \right) = 0. \quad (2.11)$$

The following is how the boundary conditions for piles with plain reinforcements are defined:

$$\begin{cases} \text{at } x = 0: & v(0, t) = 0, \frac{\partial^2 v(0, t)}{\partial x^2} = 0. \\ \text{at } x = L: & v(L, t) = 0, \frac{\partial^2 v(L, t)}{\partial x^2} = 0. \end{cases} \quad (2.12)$$

When examining the stability of dynamic variables, Equation (2.11) is one based on partial differential equations (PDE) that better to be transformed into an ordinary differential equation (ODE) for studying the stability. To do this, we approach  $v(x, t)$  in the following manner:

$$v(x, t) = \sum_{i=1}^{\infty} q_i(t) \phi_i(x), \quad \phi_i(x) = \sin \frac{i\pi x}{L} \quad (i = 1, 2, \dots). \quad (2.13)$$

In this instance, the expressions  $\phi_i(x)$  represent the orthogonal modality functions of a singly maintained column that satisfies the requirements stated in Equation (2.12).

$$\int_0^L \phi_i(x) \phi_j(x) dx = \begin{cases} 0, & i \neq j, \\ \frac{1}{2}L, & i = j. \end{cases} \quad (2.14)$$

The result that follows is as such:

$$EI \sum_{i=1}^{\infty} q_i(t) \left( \frac{i\pi}{L} \right)^4 \sin \left( \frac{i\pi x}{L} \right) - P(t) \times \sum_{i=1}^{\infty} q_i(t) \left( \frac{i\pi}{L} \right)^2 \sin \left( \frac{i\pi x}{L} \right) + \rho A \sum_{i=1}^{\infty} \ddot{q}_i(t) \sin \left( \frac{i\pi x}{L} \right) + \left( k_s \sum_{i=1}^{\infty} q_i(t) \sin \left( \frac{i\pi x}{L} \right) + c_s \sum_{i=1}^{\infty} \dot{q}_i(t) \sin \left( \frac{i\pi x}{L} \right) \right) = 0. \quad (2.15)$$

The subsequent result is obtained by multiplying Equation (2.15) by  $\Phi_n(x) = \sin \left( \frac{n\pi x}{L} \right)$  incorporating the equation across the spectrum of  $x$  from 0 to  $L$ , and using the orthogonality assumption as stated in Equation (2.14).

$$EI q_n(t) \left( \frac{n\pi}{L} \right)^4 - P(t) \times q_n(t) \left( \frac{n\pi}{L} \right)^2 + \rho A \ddot{q}_n(t) + \left( k_s q_n(t) + c_s \dot{q}_n(t) \right) = 0.$$

$$\rho A \ddot{q}_n(t) + c_s \dot{q}_n(t) + \left[ EI \left( \frac{n\pi}{L} \right)^4 - P(t) \times \left( \frac{n\pi}{L} \right)^2 + k_s \right] q_n(t) = 0. \quad (2.16)$$

### 2.2.1 Dynamic load with one frequency

One needs to consider the dynamic axial strain with the period  $T = \frac{2\pi}{\theta}$  being identical to:

$$P(t) = P_s + P_d \cos \theta t. \quad (2.17)$$

The axial pressure transmitted to the pile is represented by  $P_s$  and  $P_d$  which accordingly stand for both static and dynamic elements. Taking into consideration the subsequent data,

$$\lambda = \frac{P_s}{P_{cr}} = \frac{P_s L^2}{\pi^2 EI}, \quad \epsilon = \frac{P_d}{P_{cr}} = \frac{P_d L^2}{\pi^2 EI}, \quad \eta = \frac{k_s L^4}{\pi^2 EI}, \quad \beta = \frac{c_s}{2\rho A} = \frac{\delta \cdot \omega}{2\pi} = \frac{\delta \Omega \sqrt{n^4 - \lambda n^2 + \eta}}{2\pi}. \quad (2.18)$$

The non-dimensional static force variable  $\lambda$ , the non-dimensional dynamic load variable  $\epsilon$ , the non-dimensional foundation stiffness parameter  $\eta$ , the damping factor  $\beta$ , and the logarithmic reduction of damping  $\delta$  are all worth mentioning in light of the information supplied. Likewise  $P_{cr}$  and  $\Omega$  represent, the natural frequency of a plainly sustained pile in the first mode and the critical Euler buckling load with the following connection:

$$P_{cr} = \frac{EI\pi^2}{L^2}, \quad \Omega = \frac{\pi^2}{L^2} \sqrt{\frac{EI}{\rho A}}. \quad (2.19)$$

Employing the dimensionless variables from Equation (2.18) and then condensing the formula results in the following:

$$\ddot{q}_n(t) + 2\beta\dot{q}_n(t) + \omega^2(1 - 2\mu\cos \theta t)q_n(t) = 0. \quad (2.20)$$

Here,

$$\omega^2 = \Omega^2(n^4 - \lambda n^2 + \eta), \quad 2\mu = \frac{\Omega^2 \epsilon n^2}{\omega^2} = \frac{\epsilon n^2}{n^4 - \lambda n^2 + \eta}. \quad (2.21)$$

With regard to displacement sensibility, the first mode is the most significant. Consequently, Equation (2.20) can be written in the following manner when  $n = 1$  and the subscript are taken out:

$$\ddot{q}(t) + 2\beta\dot{q}(t) + \omega^2(1 - 2\mu\cos \theta t)q(t) = 0. \quad (2.22)$$

Here,

$$\omega^2 = \Omega^2(1 - \lambda + \eta), \quad \beta = \frac{\delta \cdot \omega}{2\pi}, \quad 2\mu = \frac{\Omega^2 \epsilon n^2}{\omega^2} = \frac{\epsilon n^2}{n^4 - \lambda n^2 + \eta}. \quad (2.23)$$

Equation (2.22) showcases the well-known damped Mathieu equation. Xie proposed a variable transformation to remove the damping term (Xie. 2006). When  $q(t) = e^{(-\beta t)}u(t)$ , the first and second derivatives of become, the renowned damped Mathieu formula is demonstrated in Equation (2.22). A factor conversion was suggested by Xie to get rid of the damping factor. The first and second variants of  $q(t)$  turn into the following when (Xie. 2006)

$$\begin{aligned} q(t) &= e^{(-\beta t)}u(t), \\ \dot{q} &= -\beta e^{(-\beta t)}u + e^{(-\beta t)}\dot{u}, \\ \ddot{q} &= \beta^2 e^{(-\beta t)}u - 2\beta e^{(-\beta t)}\dot{u} + e^{(-\beta t)}\ddot{u}. \end{aligned} \quad (2.24)$$

Substituting equation (2.24) into (2.22) to get the following standard representation of the undamped Mathieu equation.

$$\begin{aligned} \beta^2 e^{(-\beta t)}u - 2\beta e^{(-\beta t)}\dot{u} + e^{(-\beta t)}\ddot{u} + 2\beta(-\beta e^{(-\beta t)}u + e^{(-\beta t)}\dot{u}) + \omega^2(1 - \\ 2\mu \cos \theta t)e^{(-\beta t)}u = 0, \\ \ddot{u} + \omega^2 \left[ \left(1 - \frac{\beta^2}{\omega^2}\right) - 2\mu \cos \theta t \right] u = 0. \end{aligned} \quad (2.25)$$

The standard representation of an undamped Mathieu equation is Equation (2.25).

### 2.2.2 Dynamic load with two frequencies

In order to take into account two dynamic frequency needs to consider the dynamic axial strain with the period  $T_1 = \frac{2\pi}{\theta_1}$ ,  $T_2 = \frac{2\pi}{\theta_2}$  being identical to:

$$\begin{aligned} P(t) &= P_s + P_{d1} \cos \theta_1 t + P_{d2} \cos \theta_2 t, \quad P_d = P_{d1} = P_{d2}, \\ P(t) &= P_s + P_d \cos \theta_1 t + P_d \cos \theta_2 t. \end{aligned} \quad (2.26)$$

The axial pressure transmitted to the pile is represented by  $P_s$ ,  $P_{d1}$  and  $P_{d2}$  which accordingly stand for both static and two dynamic elements.

Employing the dimensionless variables from Equations (2.18, 2.19) and then condensing the formula results in the following:

$$\ddot{q}_n(t) + 2\beta \dot{q}_n(t) + \omega^2 [1 - 2\mu(\cos \theta_1 t + \cos \theta_2 t)] q_n(t) = 0, \quad (2.27)$$

Here,

$$\omega^2 = \Omega^2(n^4 - \lambda n^2 + \eta), \quad 2\mu = \frac{\Omega^2 \epsilon n^2}{\omega^2} = \frac{\epsilon n^2}{n^4 - \lambda n^2 + \eta}. \quad (2.21)$$

With regard to displacement sensibility, the first mode is the most significant. Consequently, Equation (2.27) can be written in the following manner when  $n = 1$  and the subscript are taken out:

$$\ddot{q}(t) + 2\beta\dot{q}(t) + \omega^2(1 - 2\mu(\cos \theta_1 t + \cos \theta_2 t))q(t) = 0, \quad (2.28)$$

Here,

$$\omega^2 = \Omega^2(1 - \lambda + \eta), \quad \beta = \frac{\delta \cdot \omega}{2\pi}, \quad 2\mu = \frac{\Omega^2 \epsilon n^2}{\omega^2} = \frac{\epsilon n^2}{n^4 - \lambda n^2 + \eta}. \quad (2.23)$$

Equation (2.28) showcases the well-known Damped Quasi Mathieu equation. This equation is identical to the one proposed by Sinha in his research, providing evidence that the final Equation (2.28) is accurate (Sharma and Sinha, 2018).

Xie proposed a variable transformation to remove the damping term by using Equation (2.24) “ $q(t) = e^{(-\beta t)}u(t)$ ” and substitute in Equation (2.28), and the result is (Xie. 2006):

$$\begin{aligned} \beta^2 e^{(-\beta t)}u - 2\beta e^{(-\beta t)}\dot{u} + e^{(-\beta t)}\ddot{u} + 2\beta(-\beta e^{(-\beta t)}u + e^{(-\beta t)}\dot{u}) + \omega^2(1 \\ - 2\mu(\cos \theta_1 t + \cos \theta_2 t))e^{(-\beta t)}u = 0, \end{aligned} \quad (2.29)$$

$$\ddot{u} + \omega^2 \left[ \left(1 - \frac{\beta^2}{\omega^2}\right) - 2\mu(\cos \theta_1 t + \cos \theta_2 t) \right] u = 0. \quad (2.30)$$

The standard representation of an Undamped Quasi Mathieu equation is Equation (2.30). This equation is identical to the one presented in Sinha’s work and has also been proposed by Zounes in their research. This consistency serves as validation for the correctness of the final equation in (2.29) (Rand and Hastings, 1995; Rand et al., 1999; Sharma and Sinha, 2018; Zounes and Rand, 1998; Zounes, 1997).

One of the innovations in our research is the implementation of the Mathieu equation for axial dynamic loads with both single and dual frequencies, specifically for pile foundations.

## 2.3 Summary

This chapter is dedicated to the meticulous modeling of pile foundations under dynamic loads, considering both single and dual frequencies. The focal point involves constructing a model of a beam supported by a Winkler foundation, incorporating a pair of frequencies in the analysis. The derivation of the equation of motion, detailed in Equation (2.11), employs equilibrium formulas and subsequently transforms the partial differential equation into an ordinary differential equation through the Galerkin technique, as demonstrated in Equation (2.16).

Further refinement of the equation takes place by transforming it into a Mathieu differential equation with a single frequency, utilizing unspecified variables Equations (2.22, 2.25). Additionally, the equation is extended to a Mathieu differential equation with two frequencies through the use of undefined variables, as elucidated in Equations (2.28, 2.29). Chapters 3 and 4 extend the academic discourse by providing estimation techniques and mathematical methods for solving the Mathieu differential equation with two frequencies. The chapter concludes by elaborating on the practical application of these mathematical tools, demonstrating how reactions to vibration aid in determining instability charts. This academic endeavor contributes to the advancement of knowledge in structural dynamics and geotechnical engineering.

## Chapter 3 Dynamic Stability by Approximate Method

### 3.1 Introduction

To comprehend the stability diagram of a pile foundation subjected to dynamic loading with two frequencies, this chapter will present the approach delineated by Zounes and Rand. It involves employing the Harmonic Balance technique to address dual-frequency excitation.

### 3.2 Dynamic Stability by Harmonic Balance Method

In this section, we introduce the method outlined by Zounes and Rand for dealing with dual-frequency excitation, utilizing the Harmonic Balance technique (Rand and Hastings, 1995; Rand et al., 1999; Zounes and Rand, 1998; Zounes, 1997). Furthermore, for an in-depth study of the stability equation under single-frequency excitation using both undamped and damped Mathieu equations, it is advisable to refer to Xie's book (Xie, 2006).

Utilizing Hill's infinite factors, as described in sources, is one way to obtain mathematical formulas for the evolution curves of Mathieu's Equation (3.1). (Byatt-Smith, 1979; Nayfeh and Mook, 2008; Magnus and Winkler, 1966)

$$\ddot{x} + (\delta + \epsilon \cos t)x = 0, \quad (3.1)$$

This method uses the Fourier series to represent the constrained values  $x(t)$  across the transition curves, which have intervals of  $2\pi$  or  $4\pi$

$$x(t) = A_0 + \sum_{k=1}^{\infty} \left[ A_k \cos\left(\frac{k}{2}t\right) + B_k \sin\left(\frac{k}{2}t\right) \right]. \quad (3.2)$$

An endless series of straightforward, uniform formulas for the parameters  $\{A_k, B_k\}$  appears by substituting the above statement into Mathieu's equation and equating variables with equal harmonics (using the idea of harmonic balancing). The infinite (Hill's) eigenvalue of the appropriate factor matrix must turn into zero for  $x(t)$  to have a reasonable answer. The transition trajectories inside the  $\delta - \epsilon$  variable domain of Mathieu's equation is tacitly defined by this criterion.

The QP Mathieu equation was successfully solved using a similar method utilizing Hill's infinite variables that aimed to develop mathematical formulations for the transition curves in the

$\delta - \omega$  parameter range (with a fixed  $\epsilon$ ). This approach is based on the assumption that the answers across transition curves take the shape shown in Equation (3.3), specifically,

$$q(t) = \sum_{a=0}^{\infty} \sum_{b=-\infty}^{\infty} \left[ A_{ab} \cos \left( \frac{a+b\omega}{2} t \right) + B_{ab} \sin \left( \frac{a+b\omega}{2} t \right) \right]. \quad (3.3)$$

When  $\omega$  is limited to rational standards,  $\omega = \frac{p}{q}$ , where  $p$  and  $q$  are positive values without any shared variables, the given conclusion has strong evidence. As even a tiny change in  $\omega$  would make it reasonable, it would appear that the inconsistency  $\omega$  of has no real effect. In addition, any irrational amount can be precisely estimated by a rational integer. The QP Mathieu equation adopts a version of Hill's Equation (3.4) in light of this restriction on  $\omega$  :

$$\ddot{q} + \left[ \delta + \epsilon \left( \cos t + \cos \frac{p}{q} t \right) \right] q = 0. \quad (3.4)$$

Considering  $\omega < 1$ , the recurrence of the stimulation component  $\epsilon \left( \cos t + \cos \frac{p}{q} t \right)$  with a period of  $T = 2\pi q$  is evident. According to the Floquet principle, only when the associated values of parameters lie on a transition curve does Hill's equation result in periodic answers with a period of either  $T$  or  $2T$ .

We can establish, with no loss of generality, that  $A_{-a,-b}$  is equal to  $A_{a,b}$  and  $B_{-a,-b}$  is equal to  $-B_{a,b}$ . To obtain approximate results, we employ a truncation of the infinite sums in Equation (3.3) and replace them with summations ranging from 0 to  $N$  for  $n$  and from  $-N$  to  $N$  for  $m$ .

For  $N = 1$ , we have: the expansion of series 3.10 is shown in Equation (3.5).

$$\begin{aligned} & A_{0,0} + A_{0,-1} \cos \left( \frac{t\omega}{2} \right) - B_{0,-1} \sin \left( \frac{t\omega}{2} \right) + A_{0,1} \cos \left( \frac{t\omega}{2} \right) + B_{0,1} \sin \left( \frac{t\omega}{2} \right) + A_{1,-1} \cos \left( \frac{1}{2} t\omega - \frac{1}{2} t \right) \\ & - B_{1,-1} \sin \left( \frac{1}{2} t\omega - \frac{1}{2} t \right) + A_{1,0} \cos \left( \frac{t}{2} \right) + B_{1,0} \sin \left( \frac{t}{2} \right) + A_{1,1} \cos \left( \frac{1}{2} t\omega + \frac{1}{2} t \right) + B_{1,1} \sin \left( \frac{1}{2} t\omega + \frac{1}{2} t \right) \end{aligned} \quad (3.5)$$

The QP Mathieu equation for  $N = 1$  considering (3.3, 3.4) and assuming  $A_{0,-1} = A_{0,1}, B_{0,-1} = -B_{0,1}$  is show in Equation (3.6).

$$\begin{aligned}
& A_{0,0}(\epsilon \cos(t) + \epsilon \cos(t\omega) + \delta) + \frac{(4\delta B_{1,0} - 2\epsilon B_{1,0} - 4\mu A_{1,0} - B_{1,0}) \sin\left(\frac{t}{2}\right)}{4} \\
& + \frac{(4\delta A_{1,0} + 2\epsilon A_{1,0} + 4\mu B_{1,0} - A_{1,0}) \cos\left(\frac{t}{2}\right)}{4} \\
& + \frac{(-\omega^2 B_{1,1} + (-4\mu A_{1,1} - 2B_{1,1})\omega - 4\mu A_{1,1} + 4\delta B_{1,1} - B_{1,1}) \sin\left(\frac{(1+\omega)t}{2}\right)}{4} \\
& + \frac{(\omega^2 B_{1,-1} + (-4\mu A_{1,-1} - 2B_{1,-1})\omega + 4\mu A_{1,-1} - 4\delta B_{1,-1} + B_{1,-1}) \sin\left(\frac{(-1+\omega)t}{2}\right)}{4} \\
& + \frac{\epsilon B_{1,1} \sin\left(\frac{t(3+\omega)}{2}\right)}{2} - \frac{\epsilon B_{1,-1} \sin\left(\frac{t(3\omega-1)}{2}\right)}{2} + \frac{\epsilon B_{1,1} \sin\left(\frac{t(3\omega+1)}{2}\right)}{2} \\
& + \frac{\epsilon A_{1,-1} \cos\left(\frac{t(3\omega-1)}{2}\right)}{2} + \frac{\epsilon A_{1,1} \cos\left(\frac{t(3\omega+1)}{2}\right)}{2} - \frac{\epsilon B_{1,-1} \sin\left(\frac{t(-3+\omega)}{2}\right)}{2} \\
& + \frac{\epsilon A_{1,1} \cos\left(\frac{t(3+\omega)}{2}\right)}{2} + \frac{\epsilon A_{1,-1} \cos\left(\frac{t(-3+\omega)}{2}\right)}{2} + \epsilon B_{0,1} \sin\left(\frac{t(-2+\omega)}{2}\right) \\
& + \epsilon A_{0,1} \cos\left(\frac{t(-2+\omega)}{2}\right) + \frac{(-8\mu A_{0,1}\omega - 2B_{0,1}\omega^2 + 8\delta B_{0,1} - 4B_{0,1}\epsilon) \sin\left(\frac{t\omega}{2}\right)}{4} \\
& + \frac{(8\mu B_{0,1}\omega - 2A_{0,1}\omega^2 + 8\delta A_{0,1} + 4A_{0,1}\epsilon) \cos\left(\frac{t\omega}{2}\right)}{4} \\
& + \frac{(4\epsilon A_{1,-1} - \omega^2 A_{1,1} + (4\mu B_{1,1} - 2A_{1,1})\omega + 4\mu B_{1,1} + A_{1,1}(4\delta - 1)) \cos\left(\frac{(1+\omega)t}{2}\right)}{4} \\
& + \frac{(4\epsilon A_{1,1} - \omega^2 A_{1,-1} + (-4\mu B_{1,-1} + 2A_{1,-1})\omega + 4\mu B_{1,-1} + A_{1,-1}(4\delta - 1)) \cos\left(\frac{(-1+\omega)t}{2}\right)}{4} \\
& + \epsilon A_{0,1} \cos\left(t + \frac{1}{2}t\omega\right) + \frac{\epsilon B_{1,0} \sin\left(t\omega + \frac{1}{2}t\right)}{2} - \frac{\epsilon B_{1,0} \sin\left(t\omega - \frac{1}{2}t\right)}{2} + \frac{\epsilon A_{1,0} \cos\left(t\omega - \frac{1}{2}t\right)}{2} \\
& + \frac{\epsilon A_{1,0} \cos\left(t\omega + \frac{1}{2}t\right)}{2} + \epsilon B_{0,1} \sin\left(\frac{3t\omega}{2}\right) + \epsilon A_{0,1} \cos\left(\frac{3t\omega}{2}\right) + \frac{\epsilon B_{1,0} \sin\left(\frac{3t}{2}\right)}{2} \\
& + \frac{\epsilon A_{1,0} \cos\left(\frac{3t}{2}\right)}{2} + \epsilon B_{0,1} \sin\left(t + \frac{1}{2}t\omega\right) = 0.
\end{aligned} \tag{3.6}$$

Because the QP Mathieu equation is zero, the coefficient of sine and cosine will be zero too. So, we have eq (1-9) will be zero too.

$$eq1: \delta A_{0,0} = 0,$$

$$eq2: 2\mu B_{0,1}\omega - \frac{1}{2}A_{0,1}\omega^2 + 2\delta A_{0,1} + A_{0,1}\epsilon = 0,$$

$$eq3: -2\mu A_{0,1}\omega - \frac{1}{2}B_{0,1}\omega^2 + 2\delta B_{0,1} - B_{0,1}\epsilon = 0,$$

$$eq4: \epsilon A_{1,1} - \frac{\omega^2 A_{1,-1}}{4} + \frac{(-4\mu B_{1,-1} + 2A_{1,-1})\omega}{4} + \mu B_{1,-1} + \frac{A_{1,-1}(4\delta - 1)}{4} = 0,$$

$$eq5: \frac{\omega^2 B_{1,-1}}{4} + \frac{(-4\mu A_{1,-1} - 2B_{1,-1})\omega}{4} + \mu A_{1,-1} - \delta B_{1,-1} + \frac{B_{1,-1}}{4} = 0,$$

$$eq6: \delta A_{1,0} + \frac{1}{2}\epsilon A_{1,0} + \mu B_{1,0} - \frac{1}{4}A_{1,0} = 0,$$

$$eq7: \delta B_{1,0} - \frac{1}{2}\epsilon B_{1,0} - \mu A_{1,0} - \frac{1}{4}B_{1,0} = 0,$$

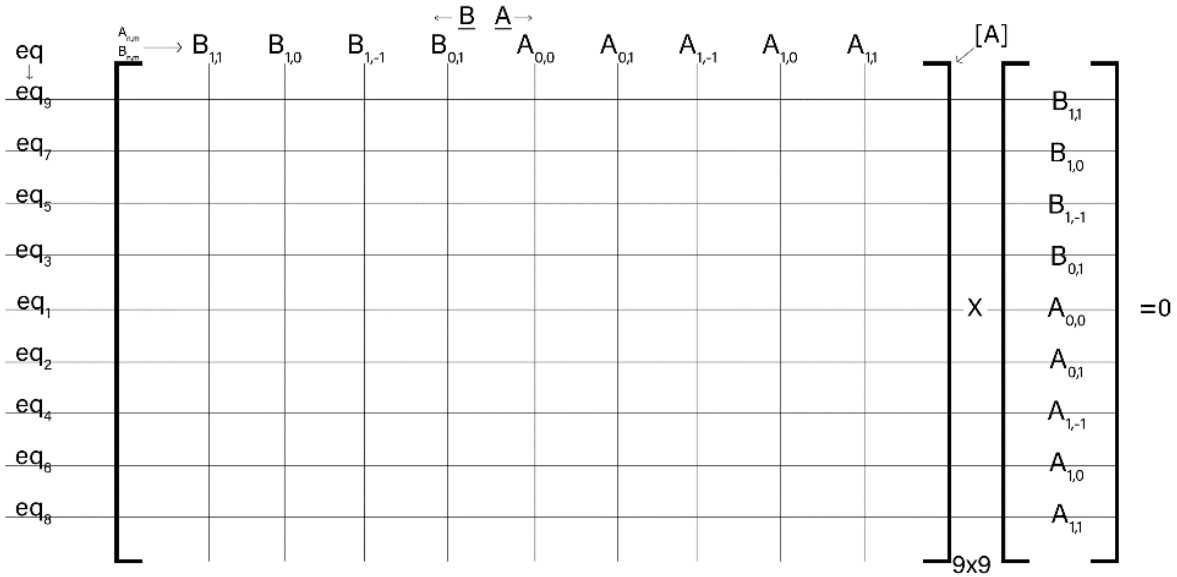
$$eq8: \epsilon A_{1,-1} - \frac{\omega^2 A_{1,1}}{4} + \frac{(4\mu B_{1,1} - 2A_{1,1})\omega}{4} + \mu B_{1,1} + \frac{A_{1,1}(4\delta - 1)}{4} = 0,$$

$$eq9: -\frac{\omega^2 B_{1,1}}{4} + \frac{(-4\mu A_{1,1} - 2B_{1,1})\omega}{4} - \mu A_{1,1} + \delta B_{1,1} - \frac{B_{1,1}}{4} = 0.$$

Rearrangement of the above nine equations into a matrix leads to

$$\begin{bmatrix} -\frac{1}{4}\omega^2 - \frac{1}{2}\omega + \delta - \frac{1}{4} & 0 & 0 & 0 & 0 & 0 & 0 & 0 & 0 & -\mu\omega - \mu \\ 0 & \delta - \frac{\epsilon}{2} - \frac{1}{4} & 0 & 0 & 0 & 0 & 0 & 0 & -\mu & 0 \\ 0 & 0 & \frac{1}{4}\omega^2 - \frac{1}{2}\omega - \delta + \frac{1}{4} & 0 & 0 & 0 & -\mu\omega + \mu & 0 & 0 & 0 \\ 0 & 0 & 0 & -\frac{\omega^2}{2} + 2\delta - \epsilon & 0 & -2\mu\omega & 0 & 0 & 0 & 0 \\ 0 & 0 & 0 & 0 & \delta & 0 & 0 & 0 & 0 & 0 \\ 0 & 0 & 0 & 2\mu\omega & 0 & -\frac{\omega^2}{2} + 2\delta + \epsilon & 0 & 0 & 0 & 0 \\ 0 & 0 & -\mu\omega + \mu & 0 & 0 & 0 & -\frac{1}{4}\omega^2 + \frac{1}{2}\omega + \delta - \frac{1}{4} & 0 & 0 & 0 \\ 0 & \mu & 0 & 0 & 0 & 0 & 0 & 0 & \delta + \frac{\epsilon}{2} - \frac{1}{4} & 0 \\ \mu\omega + \mu & 0 & 0 & 0 & 0 & 0 & \epsilon & 0 & 0 & -\frac{1}{4}\omega^2 - \frac{1}{2}\omega + \delta - \frac{1}{4} \end{bmatrix} \times \begin{bmatrix} B_{1,1} \\ B_{1,0} \\ B_{1,-1} \\ B_{0,-1} \\ A_{0,0} \\ A_{0,1} \\ A_{1,-1} \\ A_{1,0} \\ A_{1,1} \end{bmatrix} = 0. \tag{3.7}$$

The methodology for creating this matrix is shown here:



By calculating the determinant of the matrix, we have:

$$\begin{aligned}
& -4\left(\frac{\omega^4}{16} + \left(\mu^2 - \frac{\delta}{2}\right)\omega^2 + \delta^2 - \frac{\epsilon^2}{4}\right)\delta\left(\delta^2 - \frac{1}{2}\delta - \frac{1}{4}\epsilon^2 + \frac{1}{16} + \mu^2\right)\left(\frac{\omega^8}{256} + \left(-\frac{1}{64} + \frac{\mu^2}{8} - \frac{\delta}{16}\right)\omega^6\right. \\
& + \left(\frac{3\delta^2}{8} + \left(\frac{1}{16} - \mu^2\right)\delta + \frac{3}{128} + \mu^4 - \frac{\mu^2}{8} - \frac{\epsilon^2}{16}\right)\omega^4 + \left(-\delta^3 + \left(\frac{1}{4} + 2\mu^2\right)\delta^2 + \left(\frac{1}{16} + 2\mu^2 + \frac{\epsilon^2}{2}\right)\delta\right. \\
& \left. - \frac{1}{64} - 2\mu^4 - \frac{\mu^2}{8} + \frac{\epsilon^2}{8}\right)\omega^2 + \left(\delta^2 + \left(-\epsilon - \frac{1}{2}\right)\delta + \mu^2 + \frac{\epsilon}{4} + \frac{1}{16}\right)\left(\delta^2 + \left(\epsilon - \frac{1}{2}\right)\delta + \mu^2 - \frac{\epsilon}{4} + \frac{1}{16}\right).
\end{aligned} \tag{3.8}$$

By assuming  $\mu = 0$ , we have:

$$\begin{aligned}
& -4\left(\frac{1}{16}\omega^4 - \frac{1}{2}\omega^2\delta + \delta^2 - \frac{1}{4}\epsilon^2\right)\delta\left(\delta^2 - \frac{1}{2}\delta - \frac{1}{4}\epsilon^2 + \frac{1}{16}\right)\left(\frac{\omega^8}{256} + \left(-\frac{1}{64} - \frac{\delta}{16}\right)\omega^6 + \left(\frac{3}{8}\delta^2\right.\right. \\
& \left. + \frac{1}{16}\delta + \frac{3}{128} - \frac{1}{16}\epsilon^2\right)\omega^4 + \left(-\delta^3 + \frac{\delta^2}{4} + \left(\frac{1}{16} + \frac{\epsilon^2}{2}\right)\delta - \frac{1}{64} + \frac{\epsilon^2}{8}\right)\omega^2 + \left(\delta^2 + \left(-\epsilon - \frac{1}{2}\right)\delta + \frac{1}{16}\right. \\
& \left. + \frac{\epsilon}{4}\right)\left(\delta^2 + \left(\epsilon - \frac{1}{2}\right)\delta + \frac{1}{16} - \frac{\epsilon}{4}\right).
\end{aligned} \tag{3.9}$$

By equating  $\mu = 0$ ,  $\omega = \frac{7}{\pi}$ ,  $\delta = \frac{a}{\pi^2}$ ,  $\epsilon = \frac{b}{\pi^2}$ , we have:

$$\begin{aligned}
& -\frac{1}{\pi^2}\left(4\left(\frac{2401}{16\pi^4} - \frac{49a}{2\pi^4} + \frac{a^2}{\pi^4} - \frac{c^2}{4\pi^4}\right)a\left(\frac{a^2}{\pi^4} - \frac{a}{2\pi^2} - \frac{c^2}{4\pi^4} + \frac{1}{16}\right)\left(\frac{5764801}{256\pi^8}\right.\right. \\
& \left. + \frac{117649\left(-\frac{1}{64} - \frac{a}{16\pi^2}\right)}{\pi^6} + \frac{2401\left(\frac{3a^2}{8\pi^4} + \frac{a}{16\pi^2} + \frac{3}{128} - \frac{c^2}{16\pi^4}\right)}{\pi^4}\right. \\
& \left. + \frac{49\left(-\frac{a^3}{\pi^6} + \frac{a^2}{4\pi^4} + \frac{\left(\frac{1}{16} + \frac{c^2}{2\pi^4}\right)a}{\pi^2} - \frac{1}{64} + \frac{c^2}{8\pi^4}\right)}{\pi^2}\right) + \left(\frac{a^2}{\pi^4} + \frac{\left(-\frac{c}{\pi^2} - \frac{1}{2}\right)a}{\pi^2} + \frac{1}{16} + \frac{c}{4\pi^2}\right)\left(\frac{a^2}{\pi^4} + \frac{\left(\frac{c}{\pi^2} - \frac{1}{2}\right)a}{\pi^2} + \frac{1}{16} - \frac{c}{4\pi^2}\right)\right).
\end{aligned} \tag{3.10}$$

The instability diagram  $\omega - \delta$  for Equation (3.9) is the same result that Zounes and Rand have got in their research for instability diagram. (Rand and Hastings, 1995; Rand et al., 1999; Zounes and Rand, 1998; Zounes, 1997). The instability diagram  $(a - b)$  for Equation (3.10) is shown in the of Figure 3.4. It is assumed that the first frequency and second frequency of the dynamic forces are  $\pi$  and 7 respectively. It is a similar result that Sinha has got in their research for instability diagram (Sharma and Sinha, 2018).

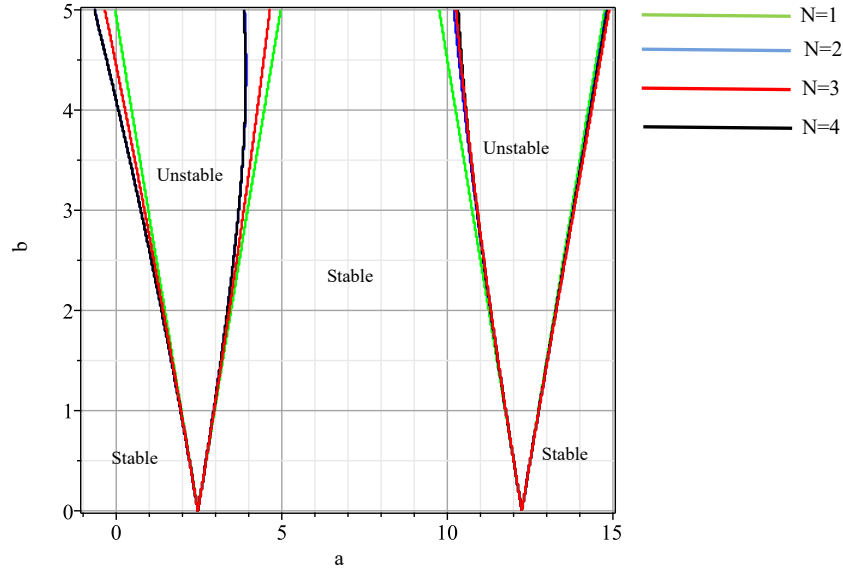


Figure 3.1 Instability Diagram - undamped –  $N$  is equal to 1 to 4.

It means that if the value of  $a$  and  $b$  is inside of the V shape, the pile will be unstable. In the following Figure 3.1,  $N$  is equal to 2 up to 4 for the undamped instability diagram ( $\omega - \delta$ ) and ( $a - b$ ). It is assumed that the first frequency and second frequency of the dynamic forces are  $\pi$  and 7 respectively for plotting ( $a - b$ ) diagram.

### 3.3 Summary

The Harmonic Balance technique is utilized to investigate the stability diagram of a pile foundation under dual-frequency dynamic loading, employing Hill's infinite variables to formulate transition curves. The resulting instability diagrams confirm the presence of instabilities within the V-shaped region. This chapter stands as a contribution to the understanding of pile foundation dynamics and the phenomena of instability under dual-frequency excitations.

## **Chapter 4 Dynamic Stability by Numerical Method**

### **A mathematical technique for calculating the motion stability of structures under two-frequency stimulation.**

#### **4.1 Introduction**

A numerical method known as the step function will be introduced to plot and discuss the stability diagram when dealing with multiple frequencies. The mathematical concept for an arrangement with multiple frequencies involves converting the two-frequency framework into a formula with only one primary frequency (period),  $T_p$ , and developing a mathematical procedure for stability under the simplified one-frequency condition.

#### **4.2 The importance of using the numerical method.**

In our rigorous academic inquiry, the Harmonic Balance method assumes a pivotal role in deciphering the complexities of the quasi-Mathieu equation, harnessing the computational prowess of the Fourier series. However, the inherent infiniteness of the Fourier series introduces approximations at each computational step, relegating the Harmonic Balance method to an approximation rather than an exact solution for the quasi-Mathieu equation. Moreover, this method involves the strategic selection of a core matrix to plot the instability region, with subsequent enlargement for improved accuracy, as elucidated in the previous chapter. This iterative process, while enhancing accuracy, still retains an element of approximation. To transcend these inherent limitations, our scholarly exploration introduces the numerical method, a precision tool meticulously applied to secure exact solutions for the intricate quasi-Mathieu equation. This methodological fusion enhances the precision of our analytical approach.

The importance of using the numerical method, as discussed in the introduction to Deng's paper, is primarily highlighted by the complexity and variability of dynamic systems under parametric excitation. These systems, which encompass a wide range of engineering applications, often involve linear second-order differential equations with periodically variable coefficients. Analytical methods like the Lyapunov, perturbation, averaging, and Floquet

methods have their limitations in accurately predicting the stability and responses of these systems. For instance, the Lyapunov method can only provide qualitative insights, and the Hill Infinite Determinant method, part of Floquet theory, faces challenges in convergence for higher order systems or those with complex excitation functions (Deng, 2023a; Deng et al., 2023).

Numerical methods address these challenges by offering a more versatile and precise approach, especially for systems where parametric excitations are not minor and cannot be neatly captured by analytical forms. This is critical in engineering, where inaccuracies in understanding the dynamic stability and responses of structures can lead to catastrophic failures. By dividing the problem into smaller segments and treating the variable coefficients as piecewise constants or linear functions, numerical methods simplify the process and enable the analysis of more complex, multi-degree-of-freedom systems. The introduction of novel numerical simulation methods, as proposed by Deng, is a testament to the evolution in this field, striving to develop comprehensive tools that can simultaneously analyze both the stability and responses of complex dynamic systems under varied parametric excitations. This progression marks a significant leap in the field of dynamic stability analysis, aligning with the need for more sophisticated and accurate tools in the face of increasingly complex engineering challenges.

### 4.3 Converting the two-frequency system into a Hill equation.

The goal is to convert an arrangement that has two different frequencies (or intervals) with a suitable one (Deng, 2023b). The main period ( $T_p$ ) is a designation given to a single period.  $T_p = K_i \cdot T_i$  ( $i = 1,2$ ), When  $K_i$  are numbers with real values, it is the least common multiple that ensures ( $T_p$ ) is an integer multiple for every value of the  $T_i$  ( $i = 1,2$ ), to minimize the time required to compute.

The commensurability of  $T_i$  determines the possibility that  $T_p$  may be attained precisely: When  $T_1$  and  $T_2$  have a reasonable proportion of the ratio  $\frac{T_1}{T_2}$ , then they are considered to be commensurable; if not, they are said to be incommensurable.

**First Case:** The precise main period  $T_p$  maybe obtained in the manner described below, provided that  $T_i$  ( $i = 1,2$ ) are commensurable.

$$T_p = \text{LCM}(T_1, T_2) = \frac{T_1 \cdot T_2}{\text{GCD}(T_1, T_2)}, \text{ for } n = 2. \quad (4.1)$$

When GCD ( $T_1, T_2$ ) is  $T_1$  and  $T_2$ 's greatest common divisor (GCD).

An Example provided here has two levels of stimulation:  $\theta_1 = \pi$ . ( $T_1 = 2$ ) and  $\theta_2 = \frac{2\pi}{3}$  ( $T_2 = 3$ ). Finding a precise  $T_p$  from Equation (4.1) is possible because  $T_1 = 2$  and  $T_2 = 3$  are commensurate.

$$T_p = \text{LCM} (T_1, T_2) = \text{LCM} (2,3) = \frac{T_1 \cdot T_2}{\text{GCD} (T_1, T_2)} = \frac{2 \cdot 3}{\text{GCD} (2,3)} = 6. \quad (4.2)$$

Therefore, a framework with one frequency,  $T_p = 6$ , and an essential angular rate,  $\theta_p = \frac{2\pi}{T_p} = \frac{\pi}{3}$ , can be used to resemble the structure of the system with two frequencies.

**The second Case:** There is no precise principal period  $T_p$  when  $T_i (i = 1,2)$  are incommensurable. Nevertheless, the subsequent reduction search procedure can be used to find the estimated essential period.

$$\Delta_2 = \min_{j=1 \dots H} \min_{k=1 \dots H} |jT_1 - kT_2|. \quad (4.3)$$

when  $\Delta_2$  is the cumulative variance and  $H$  is a suitable positive integer that determines which pair of  $(j, k)$  will result in  $\Delta_2$ . The integer value of  $|jT_1 - kT_2|$  needs to be as low as feasible, i.e., less than a minuscule stated actual number like  $10^{-2}$  so as to represent the structure of a system with two frequencies by a system with a single frequency as precisely as attainable. Throughout the search procedure, one ought to raise  $H$  and try once more if the initial value is not fulfilled. The goal of Equation (4.3) reduction is to find the ideal  $(j, k)$ . The last approximate principal period is

$$T_p = \frac{jT_1 + kT_2}{2}. \quad (4.4)$$

For the second example, it is to follow this instruction:

$$\ddot{q} + d\dot{q} + [a + b_1 \cos(\pi t) + b_2 \cos(7t)]q = 0. \quad (4.5)$$

Having been noted in Section 3, a structure that includes two frequencies,  $\theta_1 = \pi (T_1 = 2)$  and  $\theta_2 = 7 (T_2 = \frac{2\pi}{7})$ , must be converted to a primary frequency in order to examine its consistency.

Eight examples of  $H$  constants exhibiting rising accuracy but falling computational performance for the primary frequency are listed in Table 4.1. For instance, when Case 5 is

allocated with  $H = 200$ , minimising Equation (4.3) results  $j = 57$  and  $k = 127$ , which together produce  $\Delta_2 = 0.005$ . The main frequency of angulation is  $\omega_p = 0.055117$ , and the primary period is  $T_p = \frac{57T_1 + 127T_2}{2} \approx 113.9974668$ . Table 4.1 demonstrates that as  $H$  increases, the amount of  $\Delta_2$  is reduced.

Table 4.1 Comparable single-period ( $\theta_1 = \pi, \theta_2 = 7$ ).

Case	H	j	k	$jT_1$	$kT_2$	$\Delta_2$	$T_p$	$\omega_p$	$\bar{\omega}_1$	$\bar{\omega}_2$
1	10	4	9	8	8.07838	0.078	8.039190555	0.7816	3.126277586	7.034124567
2	20	9	20	18	17.9520	0.048	17.97597902	0.3495	3.145790708	6.990646018
3	50	22	49	44	43.9823	0.018	43.99114858	0.1428	3.142224771	6.998591533
4	120	35	78	70	70.01264	0.013	70.00631815	0.08975	3.141309121	7.000631752
5	<b>200</b>	<b>57</b>	<b>127</b>	<b>114</b>	<b>113.9949</b>	<b>0.005</b>	<b>113.9974668</b>	<b>0.05512</b>	<b>3.141662466</b>	<b>6.999844438</b>
6	350	149	332	298	298.0025	0.003	298.0012516	0.02108	3.141579459	7.000029402
7	800	355	791	710	709.99994	0.00006	709.99997	0.008849	3.141592786	6.999999702
8	3000	355	791	710	709.99994	0.00006	709.99997	0.008849	3.141592786	6.999999702

It is anticipated that the precision of the quantitative approach will improve as  $T_p$  increased. A higher  $T_p$ , however, would necessitate an extended calculation period. The trade-off involving  $T_p$  and processing time exists. Since Case 5 of Table 1 shows that the split endpoints merge,  $T_p = 113.9974668$ ,  $\theta_p = \frac{2\pi}{T_p} = \frac{2\pi}{113.9974668} = 0.05511688535$  can be utilized for studying dynamic stability.

#### 4.4 Computational Algorithm: Step Function

One can take into consideration the subsequent undamped Mathieu-Hill calculation (Xie, 2006) since the damped Mathieu-Hill formulas provided in Equation (2.22). can be transformed into a comparable undamped solution in Equation (2.25). This section was proposed by Deng (Deng et al., 2023).

$$\frac{d^2q(t)}{dt^2} + \omega_0^2[1 - 2\mu\Phi(t)]q(t) = 0, \quad t_0 \leq t < t_0 + T. \quad (4.6)$$

In which  $\Phi(t)$  is a periodical function for period  $T$ ,  $t_0$  is the starting point of the cycle in the structure, typically  $t_0 = 0$ ,  $\omega_0$  is the natural frequency,  $\mu$  is the amplitude of the excitation, and  $q(t)$  is the state parameter.

$$\Phi(t) = \Phi(t + T). \quad (4.7)$$

Equation (4.6) is known as the Mathieu equation provided  $\Phi(t)$  is a sinusoidal cyclic variable. If  $\Phi(t)$  is an infinite cyclic variable as it occurs more frequently, then Equation (4.6) is referred to as the Hill formula. The Step Function (or staircase function) can be used to estimate the value of the coefficient function,  $A(t) = \omega_0^2[1 - 2\mu\Phi(t)]$ , after dividing the stimulation period  $T$  into  $m$  equally spaced intervals as illustrated in Figure 4.1. Enumerating  $m = 100$  identical gaps might produce sufficiently exact outcomes. (Richards, 1975; Deng, 2021)

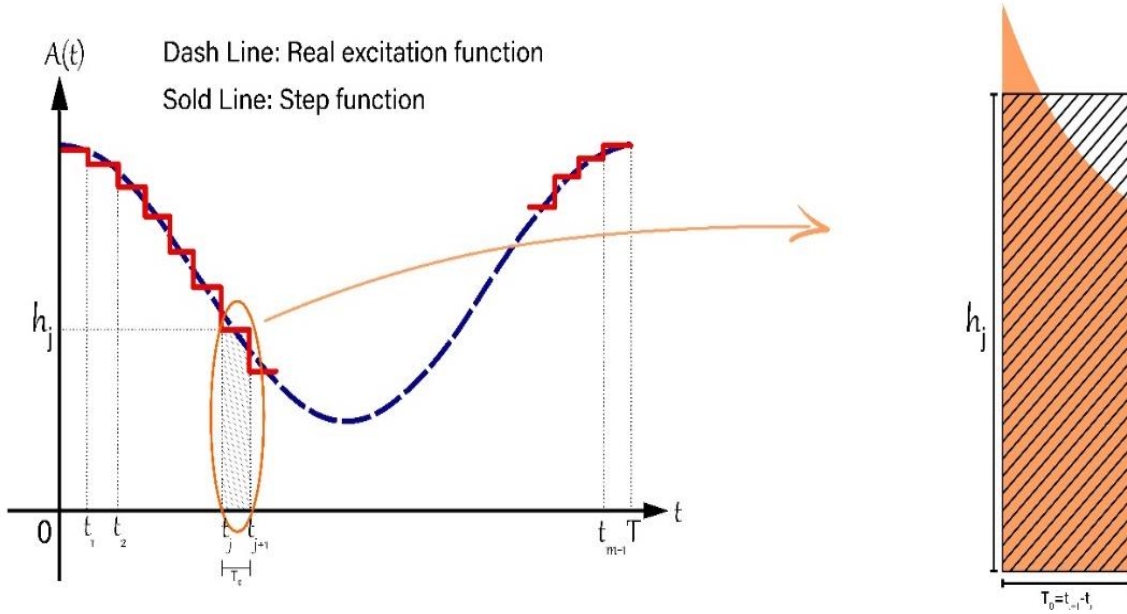


Figure 4.1 Parametric stimulation approximated behavior using step functions.

Assuming the mean elevation of  $A(t)$  is used to calculate the step function on the length of the interval  $[t_j, t_{j+1}]$ ,

$$h_j^2 = \frac{1}{T_0} \int_{t_j}^{t_{j+1}} A(t) dt = \frac{1}{T_0} \int_{t_j}^{t_{j+1}} \omega_0^2 (1 - 2\mu\Phi(t)) dt, \quad T_0 = \frac{T}{m}. \quad (4.8)$$

Consequently, the estimated value of Equation (4.6) is

$$\frac{d^2 q(t)}{dt^2} + h_j^2 q = 0, \quad t_j \leq t \leq t_{j+1}, \quad T_0 = t_{j+1} - t_j, \quad j = 0, 1, 2, \dots, m-1. \quad (4.9)$$

Wherein the unique feature of the formula is located:

$$\lambda^2 + h_j^2 = 0. \quad (4.10)$$

The overall response to Equation (4.9) is  $\lambda_{1,2} = \pm ih_j$ , in which  $i = \sqrt{-1}$  as the eigenvalues are just one set of combined number sequences.

$$q(\tau) = C_1 \sin(h_j \tau) + C_2 \cos(h_j \tau), \quad \tau = t - t_j. \quad (4.11)$$

Equation (4.11) can be expressed in a matrix structure provided the starting points,  $q(t_j)$  and  $\dot{q}(t_j)$ ,

$$\begin{bmatrix} q(\tau) \\ \dot{q}(\tau) \end{bmatrix} = \begin{bmatrix} \sin(h_j \tau) & \cos(h_j \tau) \\ h_j \cos(h_j \tau) & -h_j \sin(h_j \tau) \end{bmatrix} \begin{bmatrix} C_1 \\ C_2 \end{bmatrix}. \quad (4.12)$$

or

$$\begin{bmatrix} q(\tau) \\ \dot{q}(\tau) \end{bmatrix} = G(\tau) \begin{bmatrix} C_1 \\ C_2 \end{bmatrix}, \quad G(\tau) = \begin{bmatrix} \sin(h_j \tau) & \cos(h_j \tau) \\ h_j \cos(h_j \tau) & -h_j \sin(h_j \tau) \end{bmatrix}. \quad (4.13)$$

In this case, the (local) beginning situation at  $t = t_j$ , determines the two variables  $C_1$  and  $C_2$ :

$$\begin{bmatrix} q(t = t_j) \\ \dot{q}(t = t_j) \end{bmatrix} = \begin{bmatrix} \sin(0) & \cos(0) \\ h_j \cos(0) & -h_j \sin(0) \end{bmatrix} \begin{bmatrix} C_1 \\ C_2 \end{bmatrix} = \begin{bmatrix} 0 & 1 \\ h_j & 0 \end{bmatrix} \begin{bmatrix} C_1 \\ C_2 \end{bmatrix}. \quad (4.14)$$

Resulting in:

$$\begin{bmatrix} C_1 \\ C_2 \end{bmatrix} = G^{-1}(0) \begin{bmatrix} q(t_j) \\ \dot{q}(t_j) \end{bmatrix} = \frac{1}{-h_j} \begin{bmatrix} 0 & -1 \\ -h_j & 0 \end{bmatrix} \begin{bmatrix} q(t_j) \\ \dot{q}(t_j) \end{bmatrix}. \quad (4.15)$$

and

$$G^{-1}(0) = \begin{bmatrix} 0 & 1 \\ h_j & 0 \end{bmatrix}^{-1} = \frac{1}{-h_j} \begin{bmatrix} 0 & -1 \\ -h_j & 0 \end{bmatrix} = \begin{bmatrix} 0 & \frac{1}{h_j} \\ 1 & 0 \end{bmatrix}. \quad (4.16)$$

The solution to Equation (4.9) can be obtained in a matrix configuration by utilizing Equation (4.12):

$$\begin{bmatrix} q(\tau) \\ \dot{q}(\tau) \end{bmatrix} = G(\tau) G^{-1}(0) \begin{bmatrix} q(t_j) \\ \dot{q}(t_j) \end{bmatrix}. \quad (4.17)$$

When  $t = t_{j+1}$ , then the results are as follows:

$$\begin{bmatrix} q(t = t_{j+1}) \\ \dot{q}(t = t_{j+1}) \end{bmatrix} = G(t_{j+1} - t_j)G^{-1}(0) \begin{bmatrix} q(t_j) \\ \dot{q}(t_j) \end{bmatrix} = [M]_j \begin{bmatrix} q(t_j) \\ \dot{q}(t_j) \end{bmatrix}. \quad (4.18)$$

Here,  $[M]_j$  is considered a  $2 \times 2$  square matrix.

$$[M]_j = G(t_{j+1} - t_j)G^{-1}(0) = G(T_0)G^{-1}(0) = \begin{bmatrix} \cos(h_j T_0) & \frac{\sin(h_j T_0)}{h_j} \\ -h_j \sin(h_j T_0) & \cos(h_j T_0) \end{bmatrix}. \quad (4.19)$$

Through the  $r^{\text{th}}$  interval  $((r-1)T_0 \leq t \leq rT_0, 0 \leq r \leq m-1)$ , the responses are as such:

$$\begin{bmatrix} q(t) \\ \dot{q}(t) \end{bmatrix} = G(t - rT_0 - t_0)G^{-1}(0)[M]_{r-1} \cdots [M]_1 [M]_0 \begin{bmatrix} q(t_0) \\ \dot{q}(t_0) \end{bmatrix}. \quad (4.20)$$

In this case the (global) starting point is  $[q(t_0), \dot{q}(t_0)]^T$ , and  $[M]_{-1} = I$  is an identifier matrix of dimension two.

By looking into the state transition matrix (STM), one can ascertain the consistency of the framework in Equation (4.6) as ensues. The result of adding up the entire step-intervals in a single period is:

$$\begin{bmatrix} q(T) \\ \dot{q}(T) \end{bmatrix} = [\mathcal{M}] \begin{bmatrix} q(t_0) \\ \dot{q}(t_0) \end{bmatrix}. \quad (4.21)$$

The STM,  $[\mathcal{M}]$ , is thus provided by:

$$[\mathcal{M}] = [\mathcal{M}]_{m-1} \cdots [\mathcal{M}]_1 [\mathcal{M}]_0 = \begin{bmatrix} \mathcal{M}_{11} & \mathcal{M}_{12} \\ \mathcal{M}_{21} & \mathcal{M}_{22} \end{bmatrix}. \quad (4.22)$$

$\mathcal{M}_{11}\mathcal{M}_{22} - \mathcal{M}_{12}\mathcal{M}_{21} = 1$  can be determined. The eigenvalues of matrix  $M$  are the roots of the following equation:

$$\begin{vmatrix} \mathcal{M}_{11} - \rho & \mathcal{M}_{12} \\ \mathcal{M}_{21} & \mathcal{M}_{22} - \rho \end{vmatrix} = 0. \quad (4.23)$$

i.e.

$$\rho^2 - (\mathcal{M}_{11} + \mathcal{M}_{22})\rho + 1 = 0, \quad (4.24)$$

$$\rho_{1,2} = \frac{\mathcal{M}_{11} + \mathcal{M}_{22}}{2} \pm \sqrt{\left(\frac{\mathcal{M}_{11} + \mathcal{M}_{22}}{2}\right)^2 - 1}. \quad (4.25)$$

Asymptotical unpredictability arises once  $\left|\frac{\mathcal{M}_{11} + \mathcal{M}_{22}}{2}\right| > 1$ , since eigenvalues are real number and one of them is greater than 1. Periodic answers can be discovered when  $\left|\frac{\mathcal{M}_{11} + \mathcal{M}_{22}}{2}\right| = 1$ ,

revealing the limits of security and unpredictability. An equilibrium system arises once  $\left| \frac{\mathcal{M}_{11} + \mathcal{M}_{22}}{2} \right| < 1$ , eigenvalues are integers with complex values, and outcomes are restricted. By adding up the outcomes across the entire prior time step intervals, one can figure out the system-specific reactions in Equation (4.6). After  $n$  periods, outcomes are:

$$\begin{bmatrix} q(nT) \\ \dot{q}(nT) \end{bmatrix} = [\mathcal{M}]^n \begin{bmatrix} q(t_0) \\ \dot{q}(t_0) \end{bmatrix}. \quad (4.26)$$

Regarding the  $(n + r)$  th interval, answers are

$$\begin{bmatrix} q(t) \\ \dot{q}(t) \end{bmatrix} = G[t - (nm + r)T_0 - t_0]G^{-1}(0)[M]_{r-1} \cdots [M]_1[M]_0 \begin{bmatrix} q(nT) \\ \dot{q}(nT) \end{bmatrix}. \quad (4.27)$$

whereas  $[M]_{-1} = I$  is the dimension of the two-identity matrix, and  $(nm + r - 1)T_0 \leq t \leq (nm + r)T_0$ ,  $0 \leq r \leq m - 1$ , where  $n$  is a fraction and  $r$  is an authentic value.

## 4.5 Summary

In Section 4.2, the focus is on converting a two-frequency system into a Hill equation for a single primary frequency (period), denoted as  $T_p$ . The process involves determining the least common multiple (LCM) to ensure  $T_p$  is an integer multiple for both frequencies ( $T_1$  and  $T_2$ ). Two cases are explored: the first case when  $T_1$  and  $T_2$  are commensurable, allowing for a precise  $T_p$  the calculation, and the second case when  $T_1$  and  $T_2$  are incommensurable, requiring an estimated essential period using a reduction search procedure. In Section 4.3, a computational algorithm using a step function is introduced for the undamped Mathieu-Hill equation. The method involves estimating the coefficient function using step functions and determining the stability through matrix calculations. The step-function approach is illustrated with examples, and the computational algorithm provides insights into dynamic stability. The chapter emphasizes the trade-off between precision and processing time, showcasing the effectiveness of the proposed method in studying dynamic stability in pile foundations with multiple frequencies.

## Chapter 5 Dynamic Stability Analysis and Vibration Responses

### 5.1 Introduction

This chapter will provide a hands-on examination of a pile foundation, investigating stability diagrams through the methodologies outlined in Chapters 3 and 4. Its goal is to employ and contrast insights derived from both the Harmonic Balance technique and the numerical approach employing step functions. The focus is on gaining a practical understanding of pile foundation stability under dynamic loading with multiple frequencies. Finally, this chapter will also investigate how parameters like elastic foundation rigidity, damping, and dynamic and static loads influence instability regions.

### 5.2 Dynamic instability regions of a pile

During axial dynamic loads, assume a simply sustained pile (pin-pin supports) with a tubular cross-section. The pile is 18 meters long ( $L$ ), 508 millimeters in diameter on the exterior, and 19 millimeters thick. The cross-sectional area ( $A$ ) is therefore  $0.029\text{m}^2$ . The mass density ( $\rho$ ) and Young's elastic modulus ( $E$ ) are  $7.8 \times 10^3\text{kg/m}^3$  and  $2.1 \times 10^{11}\text{N/m}^2$ , respectively. The tubular cross-section's moment of inertia is equal. The used example assumed by Shahroudi (2023) in his thesis,

$$I = \pi \times \left( \frac{508-19}{2} \times 10^{-3} \right)^3 \times (19 \times 10^{-3}) = 8.72 \times 10^{-4}\text{m}^4. \quad (5.1)$$

Equation (2.19) states that the Euler buckling load and the pile's fundamental frequency are

$$P_{cr} = EI \left( \frac{\pi}{L} \right)^2 = 2.1 \times 10^{11} \times 8.72 \times 10^{-4} \times \left( \frac{\pi}{18} \right)^2 = 5.5781 \text{ MN}, \quad (5.2)$$

$$\Omega = \left( \frac{\pi}{L} \right)^2 \sqrt{\frac{EI}{\rho A}} = \left( \frac{\pi}{18} \right)^2 \sqrt{\frac{2.1 \times 10^{11} \times 8.72 \times 10^{-4}}{7.8 \times 10^3 \times 0.029}} = 27.4079 \frac{\text{rad}}{\text{s}} = 4.36 \text{ Hz}, \quad (5.3)$$

Then the natural period is  $T_0 = 2\pi/\Omega = 0.0697\text{s}$ . Then, the dimensionless base rigidity value could be provided by Equation (2.23)

$$\eta = \frac{k_s L^4}{\pi^2 EI} = \frac{k_s \times 18^4}{\pi^2 \times 2.1 \times 10^{11} \times 8.72 \times 10^{-4}} = 0.00005808. \quad (5.4)$$

Demonstrated below is the formula for the movement of the pile (Winkler's foundation) regarding the values mentioned before.

$$\ddot{q} + 2\beta_W \dot{q} + \omega_W^2 \left(1 - 2 \frac{\epsilon}{2(1-\lambda+\eta)} (\cos t + \cos \theta_p t)\right) q = 0. \quad (5.5)$$

In which, considering Equation (2.23),

$$\omega_W^2 = \Omega^2 (1 - \lambda + \eta) = 27.4079^2 \times (1 - \lambda + \eta) = 751.2 \times (1 - \lambda + \eta). \quad (5.6)$$

$$\beta_W = \frac{\delta \cdot \omega_W}{2\pi} = 4.36 \times \delta \sqrt{1 - \lambda + \eta}, \quad 2\mu_W = \frac{\epsilon}{1-\lambda+\eta}. \quad (5.7)$$

Here, the dimensionless dynamic load factor is represented by  $\epsilon$  whereas the dimensionless static load factor is represented by  $\lambda$ . moreover, the coefficient of damping logarithm reduction is shown by  $\delta$ .

Fundamental principles for the dimensionless base variables  $\eta$  and  $\delta$  are obtained through an analysis of the material characteristics of the soil-encircling pile. According to Richart (1970), the spectrum  $0.1 \leq \eta \leq 10$ ,  $0.05 \leq \delta \leq 0.8$  are reasonable for soil bases. In this work, we take into account  $0.5 \leq \eta \leq 4$ ,  $0.1 \leq \delta \leq 0.4$  (Engel. 1991). In this research It is assumed that  $\eta = 0.5$ ,  $\delta = 0.2$ , and  $\lambda = 0.5$  according to this assumption  $\omega_W^2$ , and  $\beta_W$  is as follows.

$$\omega_W^2 = 751.1949, \quad \beta_W = 0.8724. \quad (5.8)$$

Equation (5.5) turns into the following if  $\eta = 0.5$ ,  $\delta = 0.2$ , and  $\lambda = 0.5$

$$\ddot{q} + 0.8724 \dot{q} + 751.1949 (1 - 751.1949 \epsilon (\cos t + \cos \theta_p t)) q = 0. \quad (5.9)$$

It is assumed that  $\theta_p = \frac{p}{q}$  considered  $p$  and  $q$  are frequencies of dynamic loads.

### 5.2.1 Dynamic instability from approximate Method (Harmonic Balance – (Hill-ID))

In Chapter 3, we have introduced a comprehensive methodology meticulously developed to address the intricate challenges associated with dual-frequency excitation. This encompassed the application of the sophisticated Harmonic Balance method, along with the application of Equation (3.3) on Equation (3.1) as elucidated in Chapter 3, systematically facilitates the generation of an instability diagram  $(\frac{\theta_p}{2\omega} - \epsilon)$ .

The analytical focus revolves around a derived equation of the form as obtained in the previous section resulting from the equation in (5.9):

$$\ddot{q} + 0.8724 \dot{q} + 751.1949 (1 - 751.1949328 \epsilon (\cos t + \cos \theta_p t)) q = 0 \quad (5.9)$$

For the systematic solution of this equation employing the Harmonic Balance method, we assume a functional form for  $q(t)$  as follows in order to Zounes, Rand, and Hasting's research and then do the Harmonic Balance steps. (Rand and Hastings, 1995; Rand et al., 1999; Zounes, and Rand, 1998; Zounes, 1997).

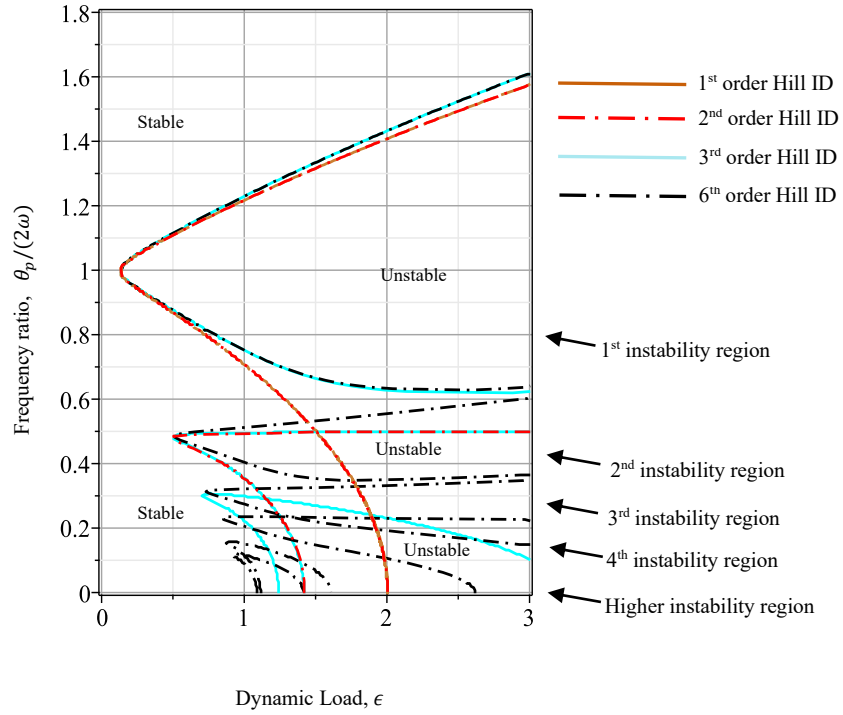
$$q(t) = \sum_{a=0}^N \sum_{b=-N}^N \left[ A_{ab} \cos \left( \frac{a+b\theta_p}{2} t \right) + B_{ab} \sin \left( \frac{a+b\theta_p}{2} t \right) \right]. \quad (5.10)$$

Under the assumption that  $N$  is equal to 6, we have constructed a coefficient matrix for sine and cosine terms, resulting in a matrix of dimensions 169 by 169. This augmented matrix provides a nuanced representation of the intricate interplay among the various harmonic components, thereby enhancing the analytical capabilities of the model. See more detail in Chapter 3. To visualize the first stability region, a systematic approach involves selecting core parameters at the center of the matrix. The core matrix, which initially started as 3 by 3 at the core and increased in dimension while maintaining a square matrix, plays a pivotal role in creating the stability regions. This process includes setting the determinant to zero and subsequently plotting the diagram  $(\frac{\theta}{2\omega} - \epsilon)$ . Expanding the core square matrix becomes imperative for plotting subsequent stability regions, where the determinant is equated to zero before the generation of corresponding diagrams. The core matrix and determinant, instrumental in creating the first stability regions, is delineated as follows.

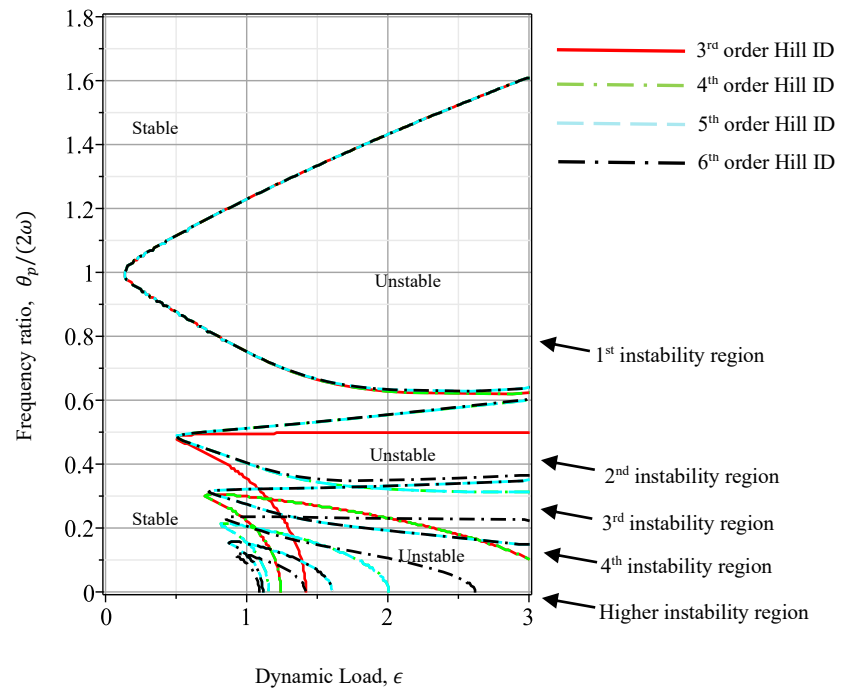
$$Ml = \begin{bmatrix} 751.1949328\epsilon - 1502.389866r^2 + 1502.389866 & 0 & -95.64510942r \\ 0 & 751.1949328 & 0 \\ 95.64510942r & 0 & -751.1949328\epsilon - 1502.389866r^2 + 1502.389866 \end{bmatrix}. \quad (5.11)$$

$$Detl := -4.238946635 \times 10^8 \epsilon^2 + 0.4\epsilon r^2 - 0.4\epsilon + 1.695578654 \times 10^9 r^4 - 3.384285387 \times 10^9 r^2 + 1.695578654 \times 10^9. \quad (5.12)$$

The outcomes of this method for first, second, third and fourth stability regions are visually presented in the subsequent figures.



(a) 1<sup>st</sup>, 2<sup>nd</sup>, 3<sup>rd</sup>, and 6<sup>th</sup> order Hill ID



(b) 3<sup>rd</sup>, 4<sup>th</sup>, 5<sup>th</sup>, and 6<sup>th</sup> order Hill ID

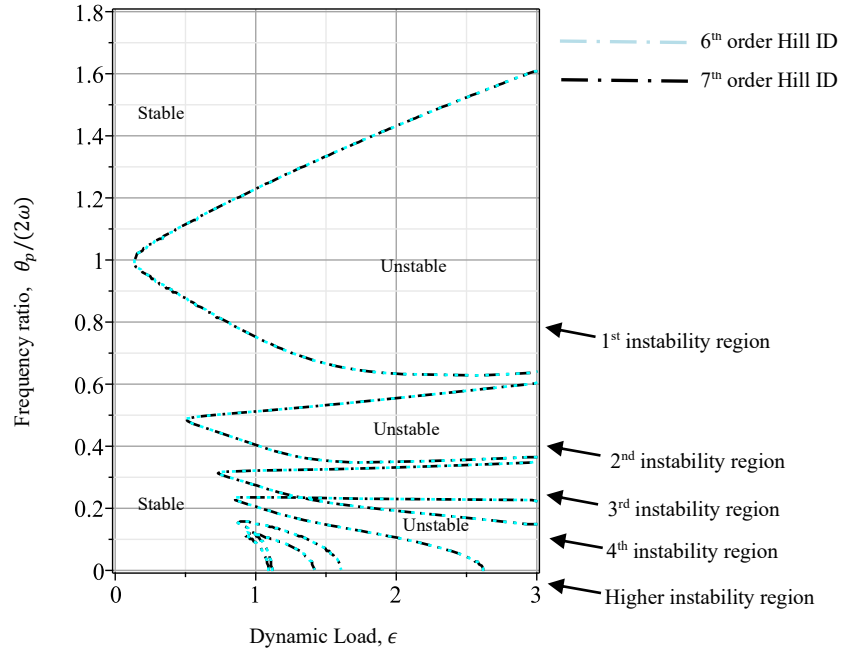
(c) 6<sup>th</sup> and 7<sup>th</sup> order Hill ID

Figure 5.1 Harmonic Balance Stability regions (Hill-ID regions).

The identified V-shaped region within the diagram signifies a crucial boundary delineating stability and instability. In the context of this analysis, the V-shaped region's interior is marked as unstable, implying those solutions within this parameter space exhibit dynamic behavior prone to instability. Conversely, points situated outside this V-shaped region are deemed stable, indicating a more predictable and controlled system response.

### 5.2.2 Dynamic instability from Numerical Method (Step Function Method)

In Chapter 4, the focus is on a numerical method for evaluating the motion stability of constructions subjected to two-frequency stimulation. The chapter introduces a systematic approach to convert a dual-frequency system into a Hill equation with a single primary frequency, utilizing the least common multiple (LCM). Two scenarios are considered: commensurable frequencies leading to a precise period ( $T_p$ ), and incommensurable frequencies requiring an estimated essential period obtained through a reduction search procedure.

The analytical focus revolves around a derived Equation (5.9) of the form below as obtained in the 5.2:

$$\ddot{q} + 0.8724216855 \dot{q} + 751.1949328 (1 - 751.1949328 \epsilon (\cos t + \cos \theta_p t))q = 0. \quad (5.9)$$

In the equation, we have:

$$\lambda = 0.5, \delta = 0.2, \eta = 0.5, \beta_W = \frac{\delta \cdot \omega_W}{2\pi} = 0.8724216855$$

$$\omega_W^2 = \Omega^2(1 - \lambda + \eta) = 751.1949328. \quad (5.13)$$

Section 4.1 calculates  $T_p$  and  $\theta_p$  using  $p = \pi$  and  $q = \frac{2\pi}{3}$  for the first example. The results are  $T_p = 6$  and  $\theta_p = \frac{2\pi}{T_p} = \frac{\pi}{3}$ .

For the second example, we assume that  $p$  and  $q$  are incommensurable which is  $\theta_1 = \pi, \theta_2 = 7$ . The results are  $T_p = 113.9974668$  and  $\theta_p = \frac{2\pi}{T_p} = \frac{2\pi}{113.9974668} = 0.05511688535$ . By this, the two-frequency change into one frequency by having  $\theta_p$ .

Subsequently, Equation (5.9) is applied with  $\theta_p = \frac{\pi}{3}$  for the first example and  $\theta_p = 0.05511688535$  for the second example. In place of  $p$  and  $q$ , transforming the equation into:

$$\ddot{q} + 0.8724216855 \dot{q} + 751.1949328 (1 - 751.1949328 \epsilon (\cos \theta_p t))q = 0. \quad (5.14)$$

$q(t) = e^{-0.8724216855/2}u(t)$  could be employed to change Equation (5.14) into a comparable undamped Mathieu equation.

$$\ddot{u} + 751.1949328 \left(1 - \frac{\epsilon}{1-\lambda+\eta} \cos \theta_p t\right) u = 0. \quad (5.15)$$

Following this modification, the Step Function Method detailed in Section 4.2 is employed to solve the equation and generate a stability diagram. Section 4.2 proposes a computational algorithm utilizing the Mathieu-Hill equation, incorporating step functions to approximate parametric stimulation behavior. Eigenvalues play a pivotal role in determining system stability, ultimately leading to the plotting of the stability diagram. Figure 5.2 depicts the stability diagram resulting from the Step Function Method.

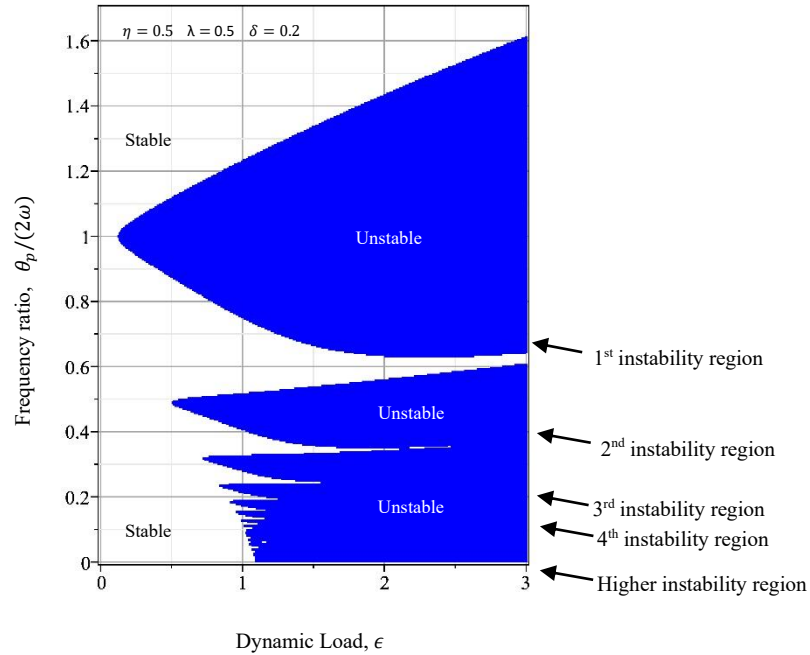
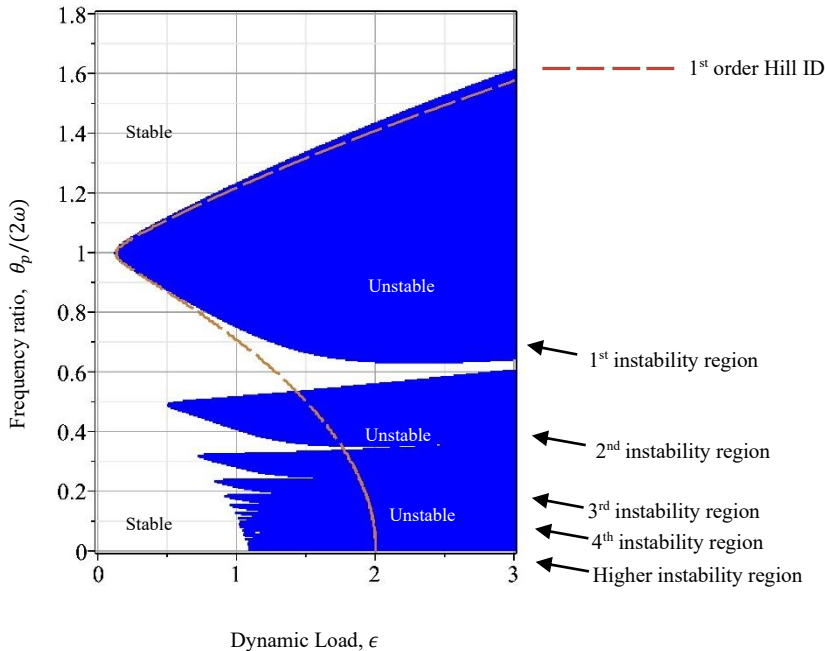


Figure 5.2 Instability regions from the numerical simulation.

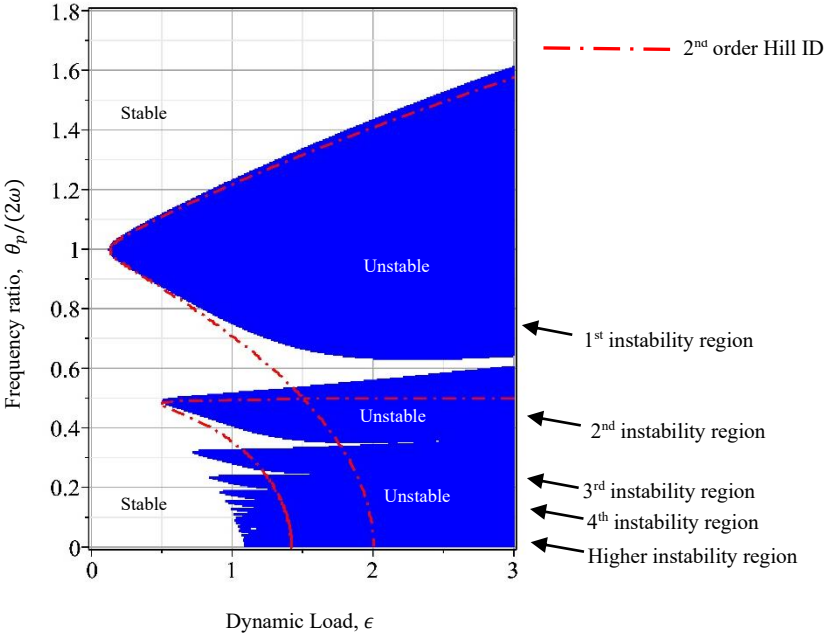
The delineated V-shaped area in the diagram represents a significant boundary demarcating stability from instability. In the context of this examination, the interior of the V-shaped region is characterized as unstable, indicating that solutions within this parameter space display dynamic behavior susceptible to instability. Conversely, points located outside this V-shaped region are considered stable, suggesting a more foreseeable and controlled system response.

### 5.3 Calibration of the result from the Harmonic Balance Method

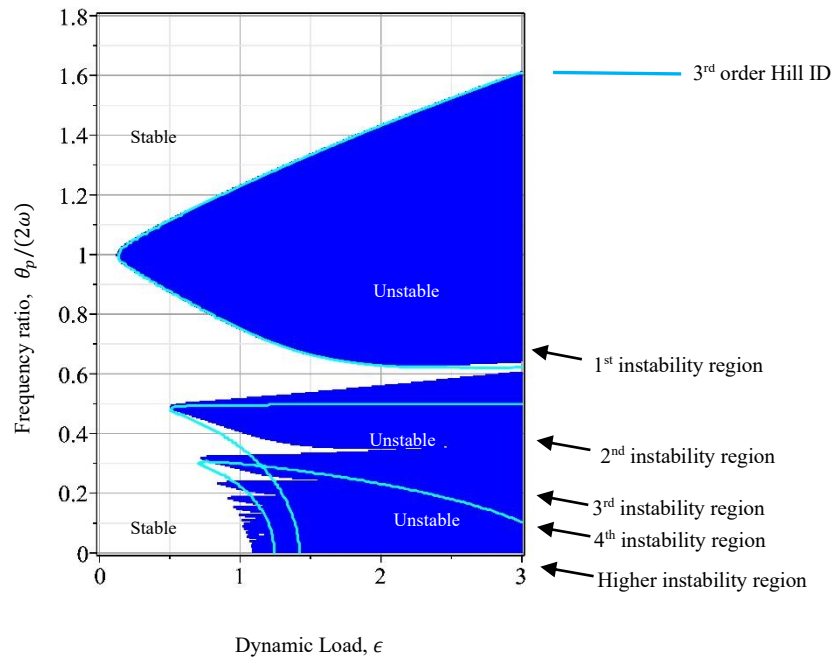
The Hill ID of the Harmonic Balance approach in Equations (5.9) and (5.10) can be utilized used to identify the instability zones of Equation (5.12). Here, both Figures 5.3 and 5.4 display the initial levels of Hill ID limitations.



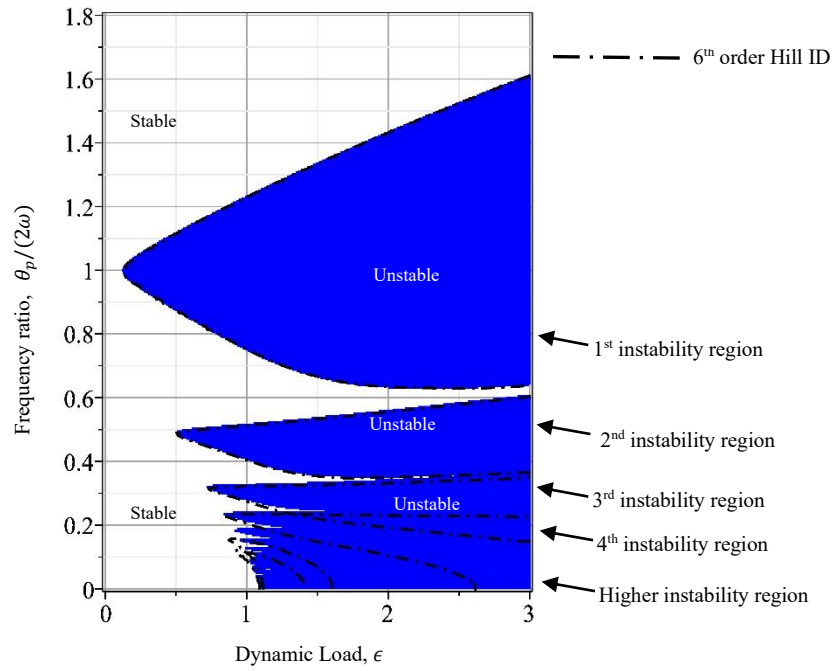
(a) Numerical result and 1<sup>st</sup> order Hill ID



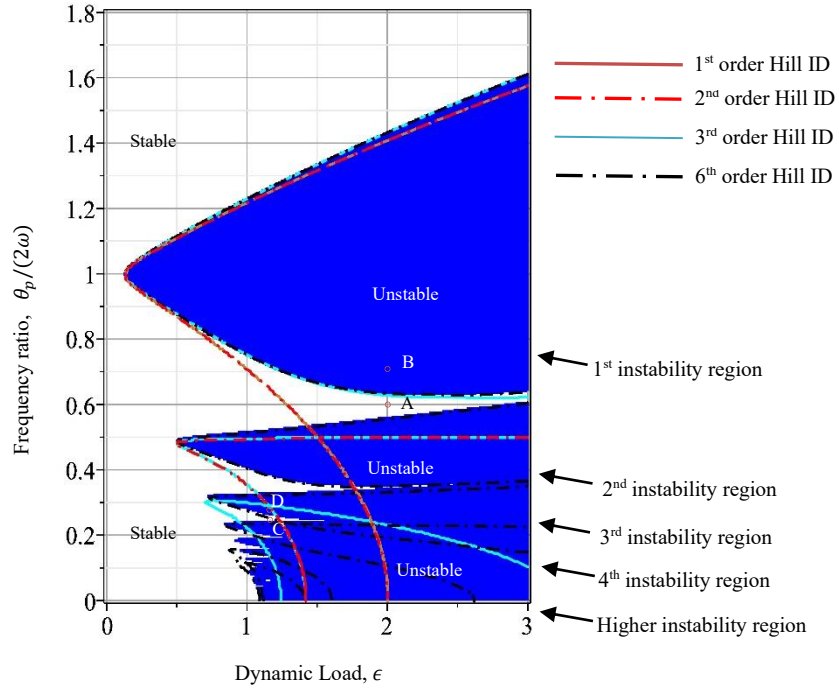
(b) Numerical result and 2<sup>nd</sup> order Hill ID



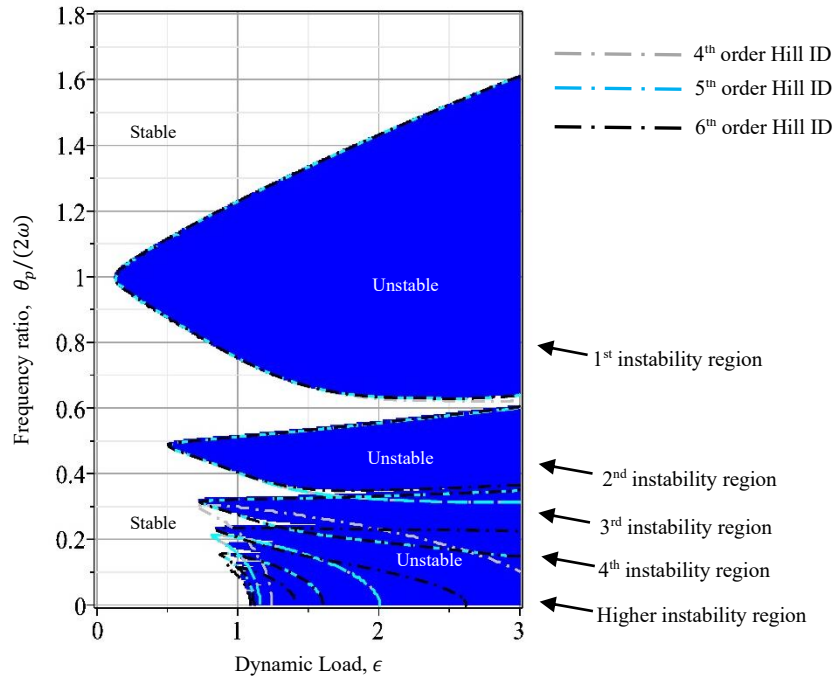
(c) Numerical result and 3<sup>rd</sup> order Hill ID



(d) Numerical result and 6<sup>th</sup> order Hill ID



(e) Numerical result and 1<sup>st</sup>, 2<sup>nd</sup>, 3<sup>rd</sup>, and 6<sup>th</sup> order Hill ID



(f) Numerical result and 4<sup>th</sup>, 5<sup>th</sup>, and 6<sup>th</sup> order Hill ID

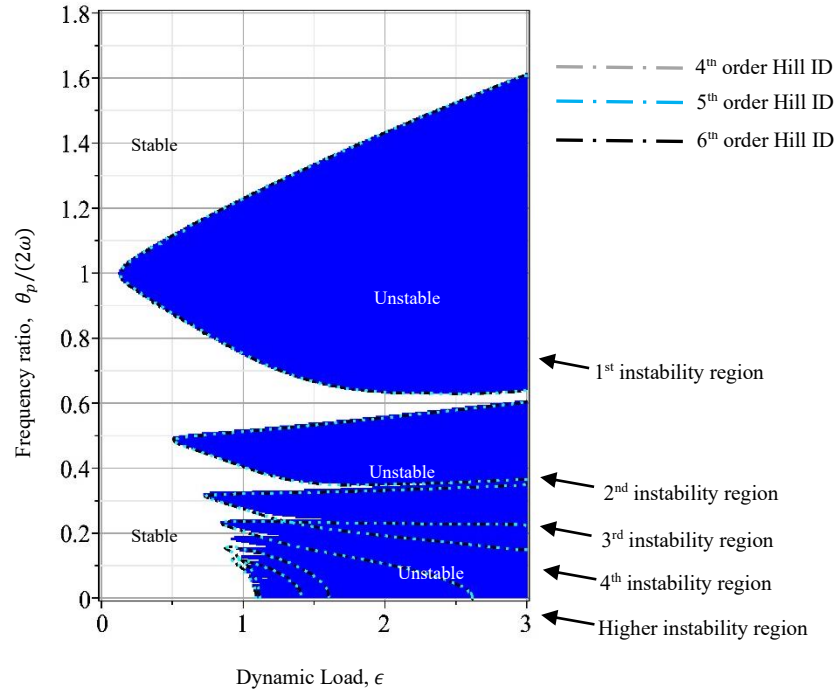
(g) Numerical result and 6<sup>th</sup>, and 7<sup>th</sup> order Hill ID

Figure 5.3 The Mathematical Simulation's Instability Zones and the orders of Hill ID.

The blue-shaded portions of Figure 5.3 represent the instability zones, leading to being statistically determined through the procedure described in Section 4.

The blank areas in these figures' unfilled zones show stability. Figure 5.3 illustrates the manner in which a border is drawn more precisely when the number of Hill ID orders that are employed increases. The second-order and third-order Hill ID limits are appropriate for the initial instability zone, while the first-order Hill ID limit is erroneous. As seen in Figure 5.4, the fourth-order Hill ID boundary is appropriate for the third instability zone, while neither of them is precise.

Four structures' reactions to vibration are examined in order to demonstrate the exactitude of our computational modeling and the Hill ID boundaries from the Harmonic Balance Method:  $A \left( \epsilon = 2, \frac{\theta_p}{2\omega_W} = 0.6 \right)$ ,  $B \left( \epsilon = 2, \frac{\theta_p}{2\omega_W} = 0.7 \right)$ ,  $C \left( \epsilon = 1.4, \frac{\theta_p}{2\omega_W} = 0.24 \right)$ , and  $D \left( \epsilon = 1.4, \frac{\theta_p}{2\omega_W} = 0.26 \right)$ . In Figure 5.3.e, the points correspond to these four dynamical structures. The starting parameters are as follows: in instances A and C,  $q(0) = 0$  and  $\dot{q}(0) = 0.1$ ; for cases B and D,

$q(0) = 0$  and  $\dot{q}(0) = 0.0001$ . Figures 5.5a and 5.5c show that as the point till repose increases, the vibration reactions of the structures at points A and C also drop, suggesting the presence of stability. This demonstrates the inaccuracy of the first-order Hill ID boundary for the first instability zone. The third-order Hill ID boundary is imprecise for the third instability region. Nonetheless, computational findings can distinguish between instability and stability with sufficient accuracy. In contrast, however, as Figures 5.5b and 5.5d demonstrate, the vibration reactions of the structures at the two locations B and D improve with time unboundedly, resulting in a state of unpredictability. The outcomes of the computational simulations are crucial measurement factor findings.

#### 5.4 Quantitative solutions for vibration reactions

The vibration reactions of Equation (5.15) can be ascertained by Equation (4.27) from the suggested algorithm since the dynamical structure in Equation (5.14) can be transformed into an undamped Mathieu formula in Equation (5.15). The standard computations of differential equations, like the Runge-Kutta approach, may confirm these vibration reactions (Xie, 2006). Using Equation (5.15) and permitting  $y_1 = q$ ,  $y_2 = \dot{q}$ , one has

$$\dot{y}_2 = -2\beta y_2 + \omega^2(1 - 2\mu(\cos t + \cos \theta_p t))y_1, \quad \theta_p = \frac{p}{q} \quad (5.16)$$

Executing the initial stage of the step function method outlined in Sections 5.1.2 and 4.1 results in the convergence of the two frequencies into one frequency, facilitated by the incorporation of  $\theta_p$ .

$$\dot{y}_2 = -2\beta y_2 + \omega^2(1 - 2\mu \cos \theta_p t)y_1. \quad (5.17)$$

in the matrix format, this could be described as the following:

$$\begin{aligned} \begin{Bmatrix} \dot{y}_1 \\ \dot{y}_2 \end{Bmatrix} &= \begin{Bmatrix} y_2 \\ -2\beta y_2 + \omega^2(1 - 2\mu \cos \theta_p t)y_1 \end{Bmatrix} = \begin{Bmatrix} f_1(t, \mathbf{y}) \\ f_2(t, \mathbf{y}) \end{Bmatrix} = \begin{Bmatrix} f_1(t; y_1, y_2) \\ f_2(t; y_1, y_2) \end{Bmatrix}, \\ \mathbf{y} &= \begin{Bmatrix} y_1 \\ y_2 \end{Bmatrix}. \end{aligned} \quad (5.18)$$

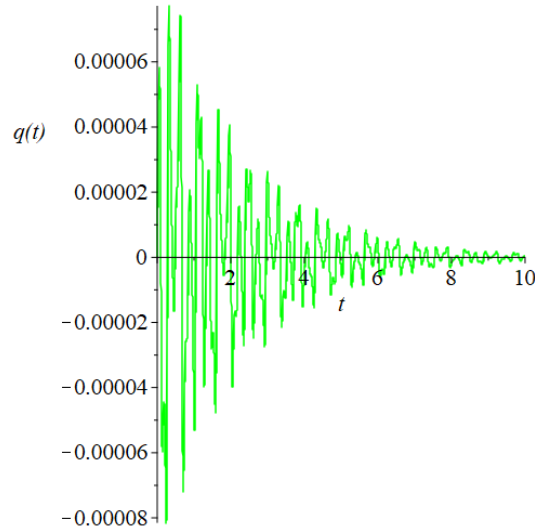
Applying Equation (5.15) to the instance of point A in Figure 5.2, one obtains the equation of motion.

$$\ddot{q} + 0.8724\dot{q} + 751.1949[1 - 2\cos(32.8895t)]q = 0, \quad (5.19)$$

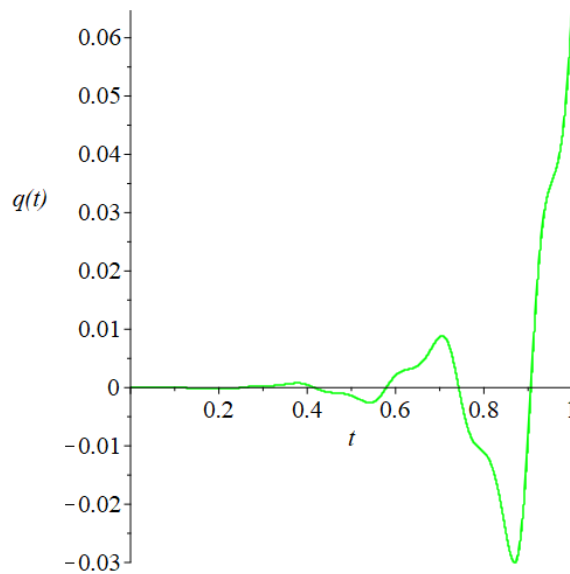
$$f_1(t; y_1, y_2) = y_2,$$

$$f_2(t; y_1, y_2) = -0.8724y_2 - 751.1949(1 - 2\cos 32.8895t)y_1. \quad (5.20)$$

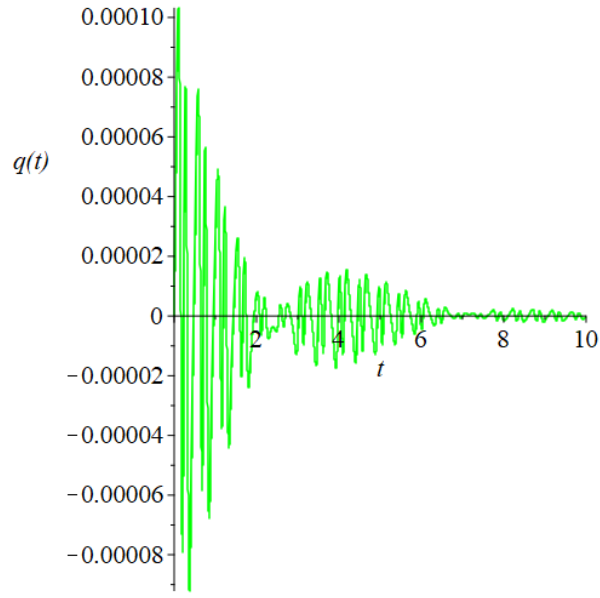
Equation (5.19) can be mathematically accomplished via the fourth-order Runge-Kutta approach. According to the starting point,  $q(t_0 = 0) = 0$  and  $\dot{q}(t_0 = 0) = 0.001$ . Figure 5.5a displays the vibration reactions' outcome. Our approach in the chapter. 4 yields computational findings that are as accurate as the fourth-order Runge-Kutta method.



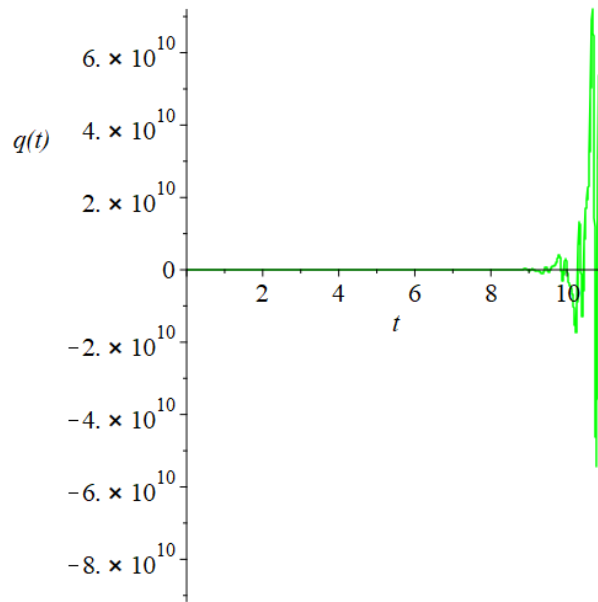
(a) point A  $\left(\epsilon = 2, \frac{\theta_p}{2\omega_W} = 0.6\right)$ .



(b) point B  $\left(\epsilon = 2, \frac{\theta_p}{2\omega_W} = 0.7\right)$ .



(c) point C  $\left(\epsilon = 1.4, \frac{\theta_p}{2\omega_W} = 0.24\right)$ .

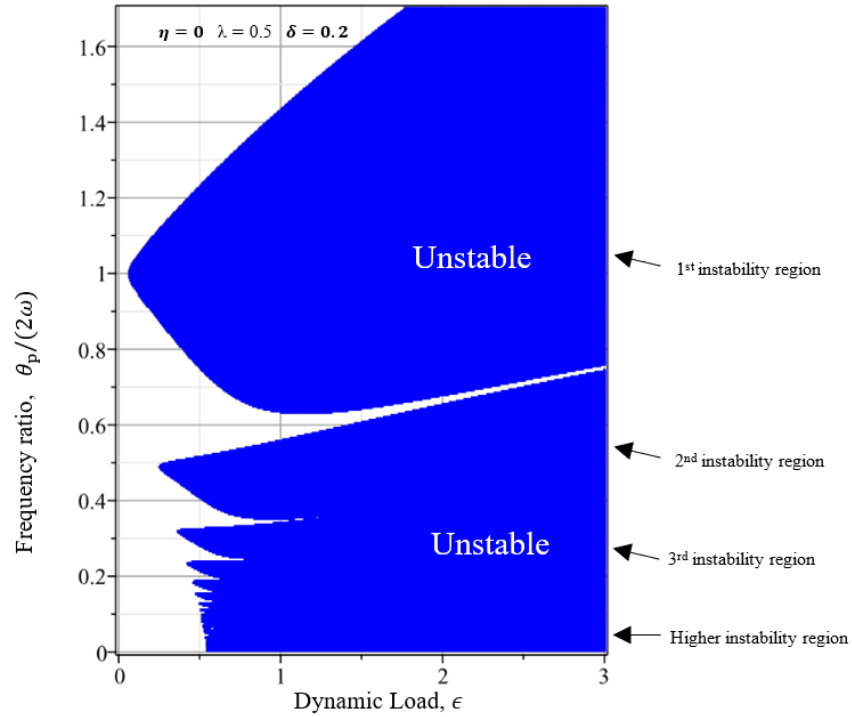


(d) point D  $\left(\epsilon = 1.4, \frac{\theta_p}{2\omega_W} = 0.26\right)$ .

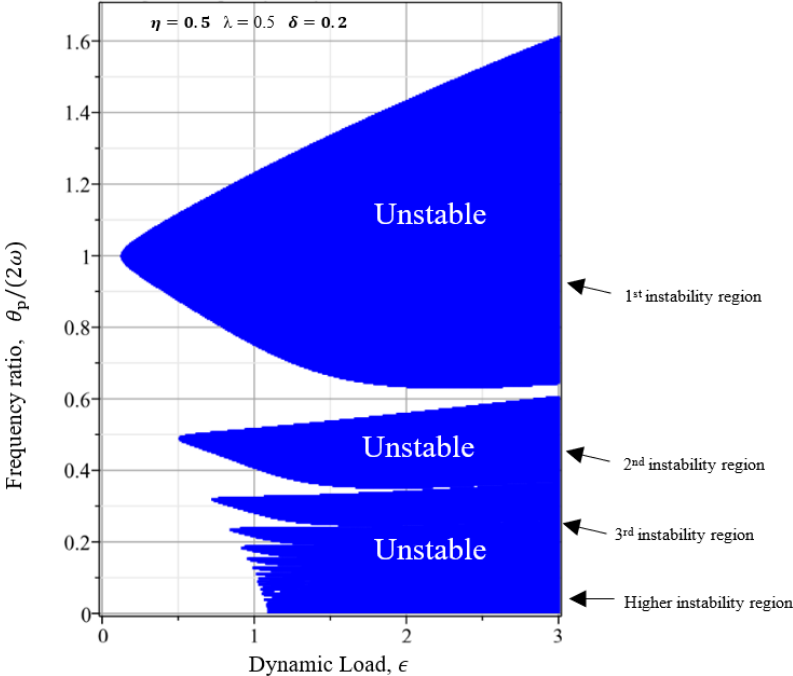
Figure 5.5 Vibration response. (Continued)

## 5.5 Impact of the Elastic Foundation

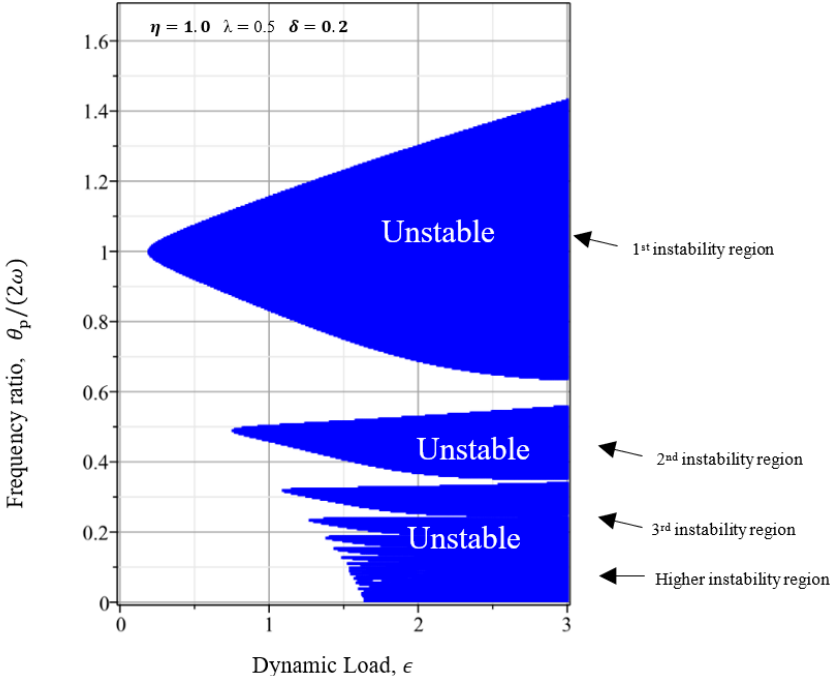
Figure 5.6 illustrates the impact of dynamic load upon the structure of instability schematics based on distinct Winkler foundation rigidity. The critical dimensionless dynamic load increases as the rigidity of the Winkler foundation expands, and the unpredictability diagram's area dramatically contracts.



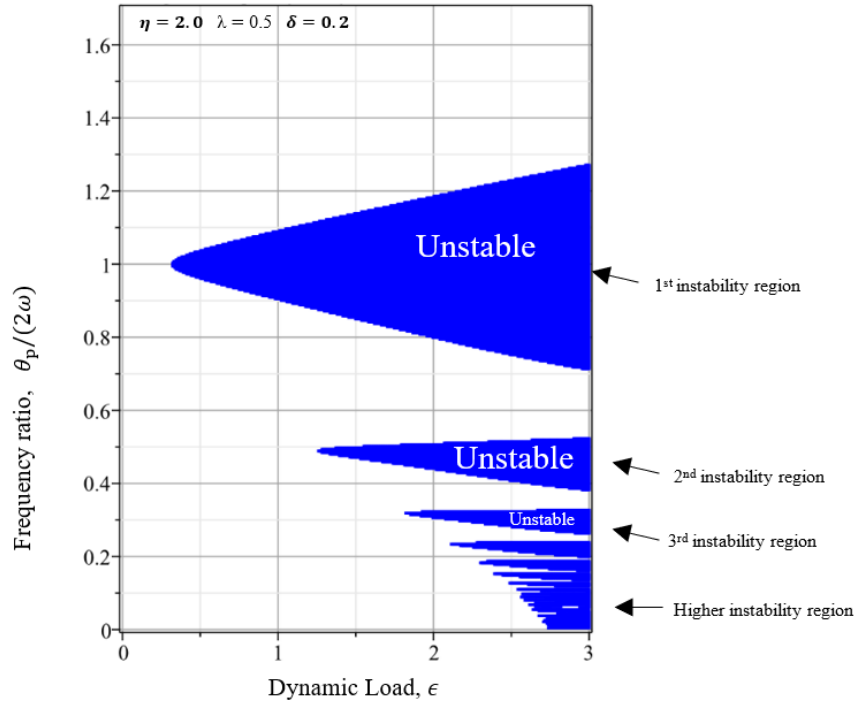
a)  $\eta = 0$   $\lambda = 0.5$   $\delta = 0.2$



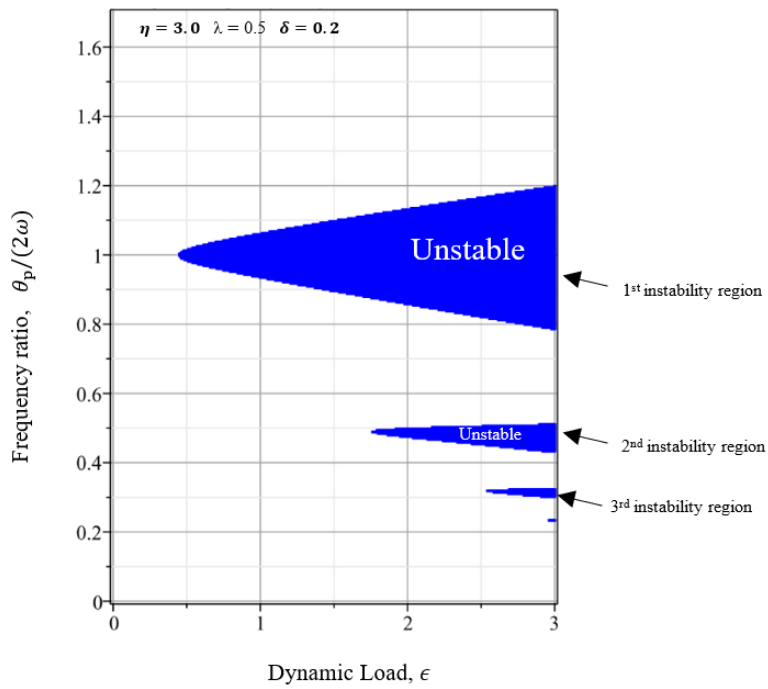
b)  $\eta = 0.5 \quad \lambda = 0.5 \quad \delta = 0.2$



c)  $\eta = 1.0 \quad \lambda = 0.5 \quad \delta = 0.2$



d)  $\eta = 2.0 \quad \lambda = 0.5 \quad \delta = 0.2$



e)  $\eta = 3.0 \quad \lambda = 0.5 \quad \delta = 0.2$

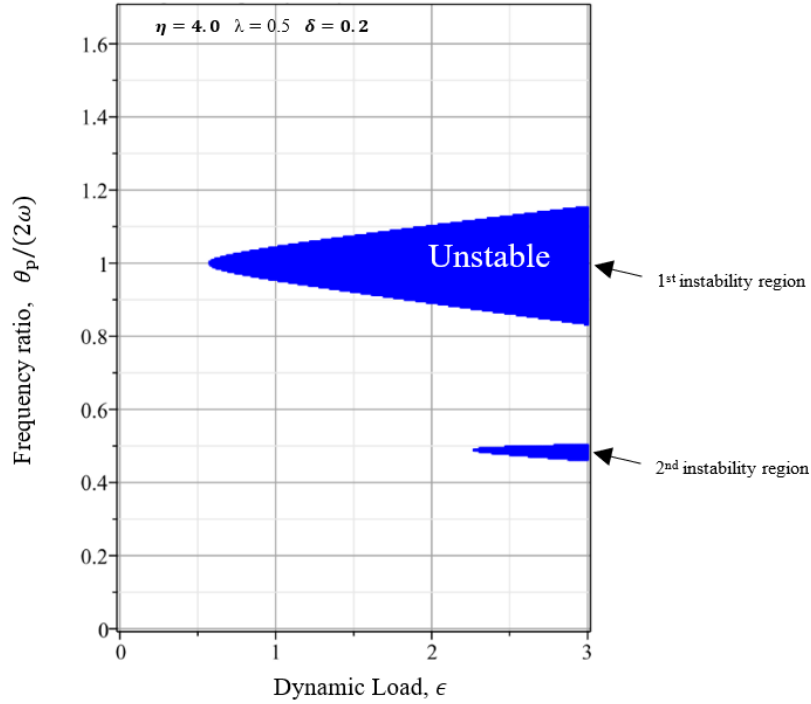
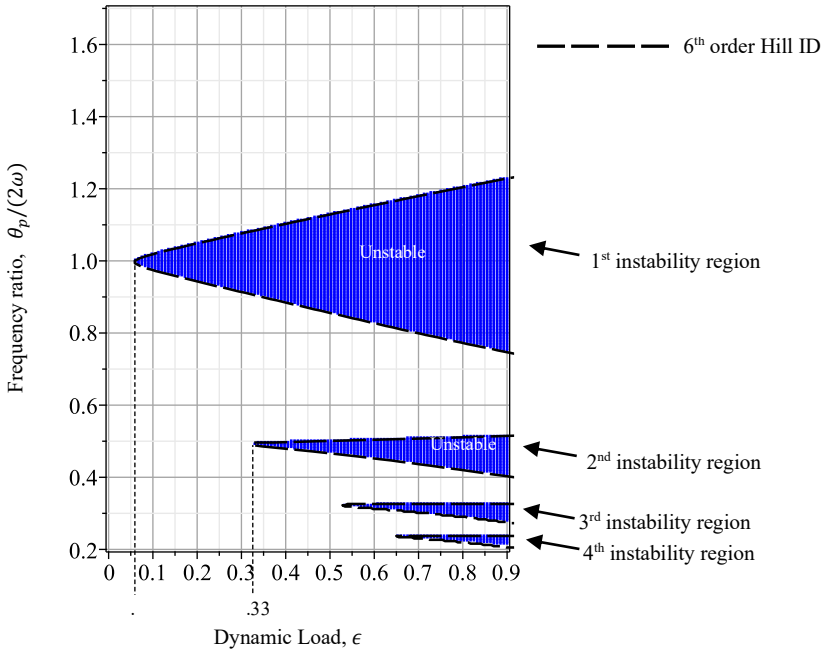
(f)  $\eta = 4.0$   $\lambda = 0.5$   $\delta = 0.2$ 

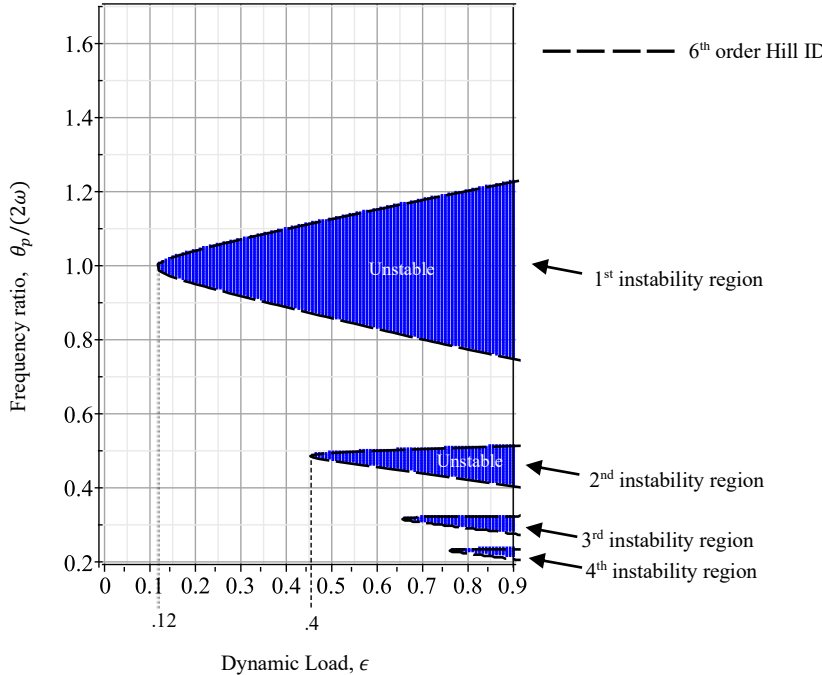
Figure 5.6 Impact of dynamic load at different foundation rigidity levels.

## 5.6 Impact of Damping

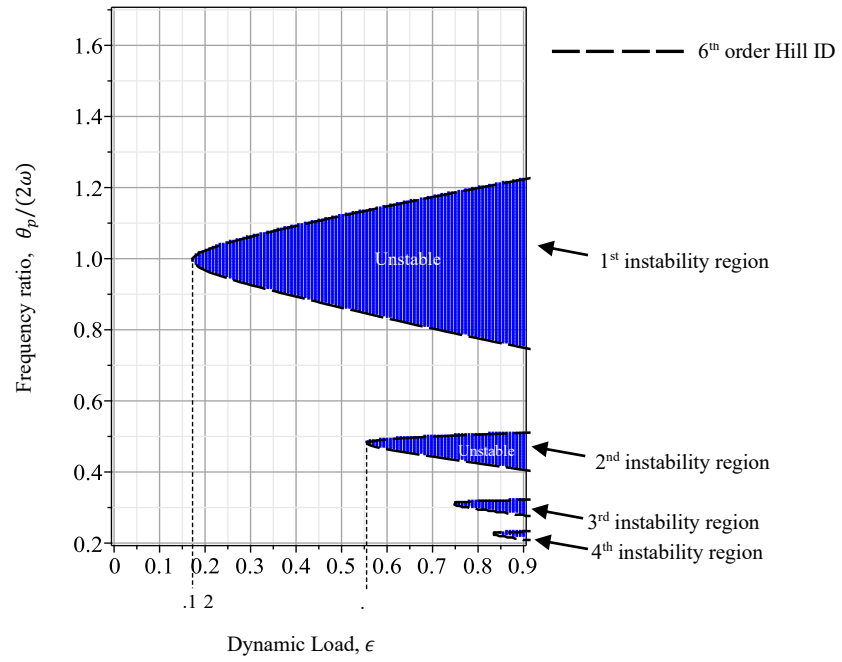
Parametric estimation resonances can happen in some situations, as shown in Figure 5.7, despite damping. The spectrum of the instability stimulation frequency gradually decreases as long as it vanishes as the foundation damping,  $\delta$ , increases. A significant dynamic element load arises for a foundation damping to cause instability, as Figure 5.7 illustrates, for both the first and second instability regions. An increased dynamic element load for instability necessitates an increased foundation damping. The most important dynamic element load rises from 0.06 to 0.23 for the first instability zone as the foundation damping shifts from  $\delta = 0.1$  to 0.4.



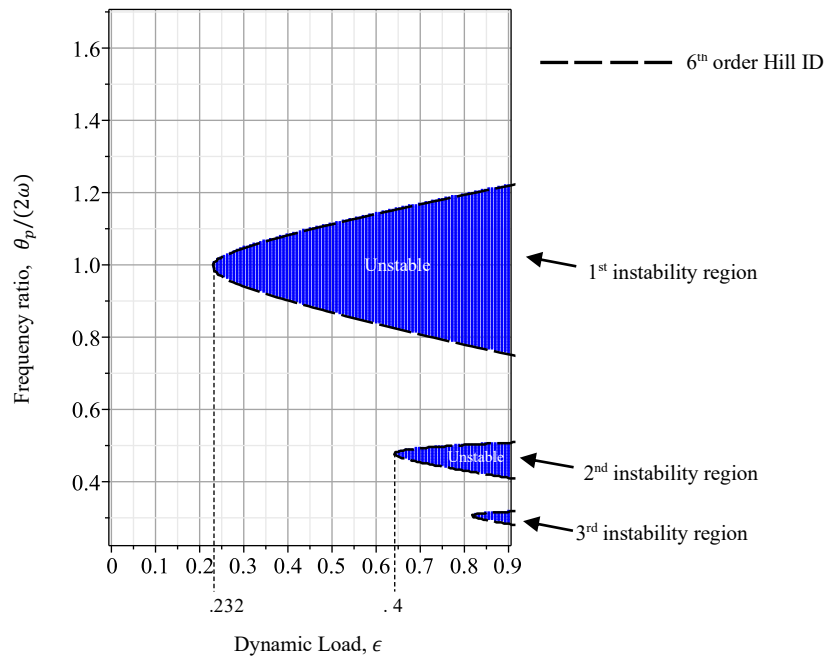
a)  $\delta = 0.1 \quad \eta = 0.1 \quad \lambda = 0.2.$



b)  $\delta = 0.2 \quad \eta = 0.1 \quad \lambda = 0.2.$



c)  $\delta = 0.3 \quad \eta = 0.1 \quad \lambda = 0.2.$



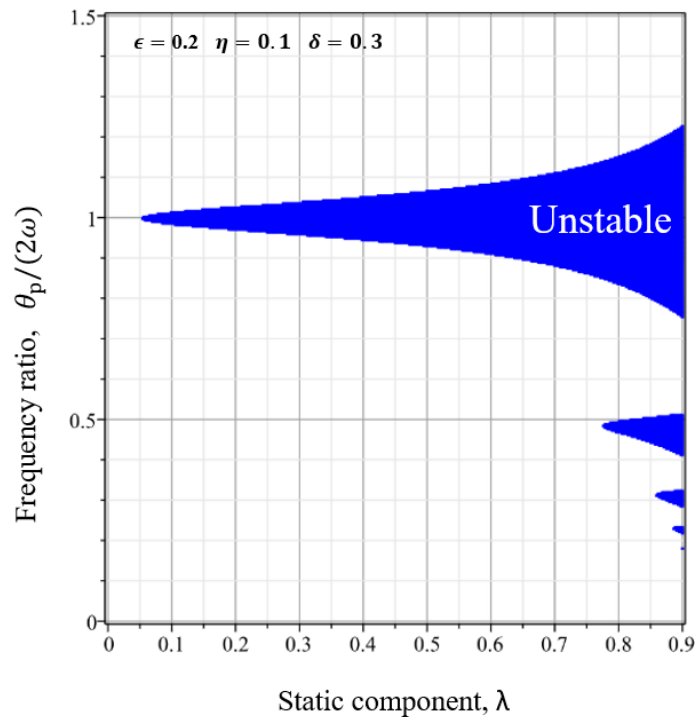
d)  $\delta = 0.4 \quad \eta = 0.1 \quad \lambda = 0.2.$

Figure 5.7 Damping Impact.

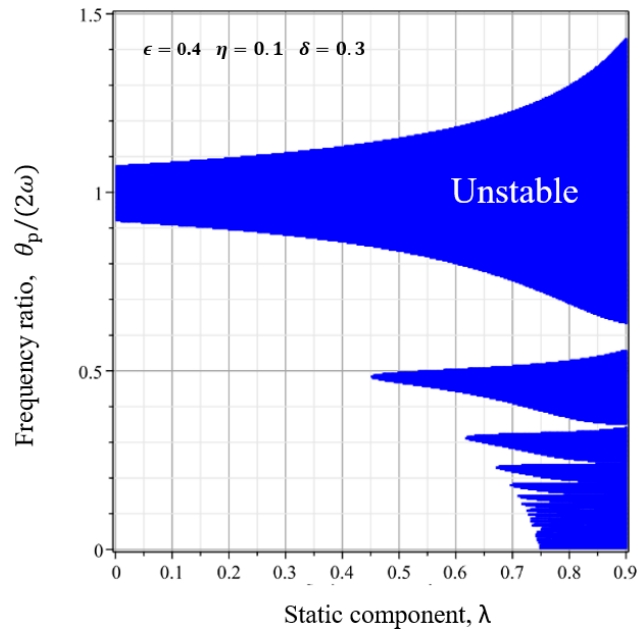
## 5.7 Impact of dynamic and static component loads

The vibrating lateral load on the pile,  $P(t)$ , which consists of a static element,  $P_s$ , and a dynamic element,  $P_d$ , with two frequencies taken into account in Equation (2.26). The dynamic element may result from an earthquake or demolition, while the static element can arise from the amount of mass of the rock layer (Deng, 2021).

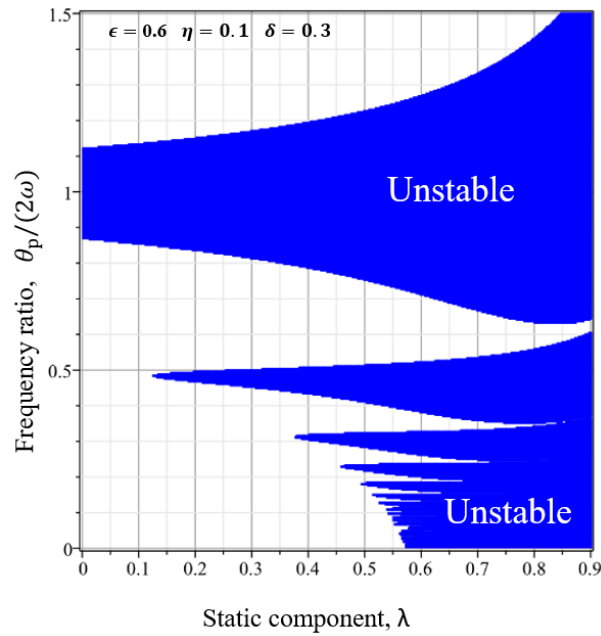
The instability graphs corresponding to various dimensionless dynamic loads  $\epsilon = 0.2, 0.4, 0.6$  are presented in Figure 5.8. The spectrum of the stimulation frequency for instability rises substantially with increasing static load. The Hill ID additionally demonstrates the perimeters of instability. As illustrated in Figure 5.8.a, there exists an essential static element to induce instability as the magnitude of the dynamic element load,  $\epsilon$ , is limited. As demonstrated in Figures 5.8b and 5.8c, a static element might not be necessary to cause instability once  $\epsilon$  increases.



a)  $\epsilon = 0.2$   $\eta = 0.1$   $\delta = 0.3$ .



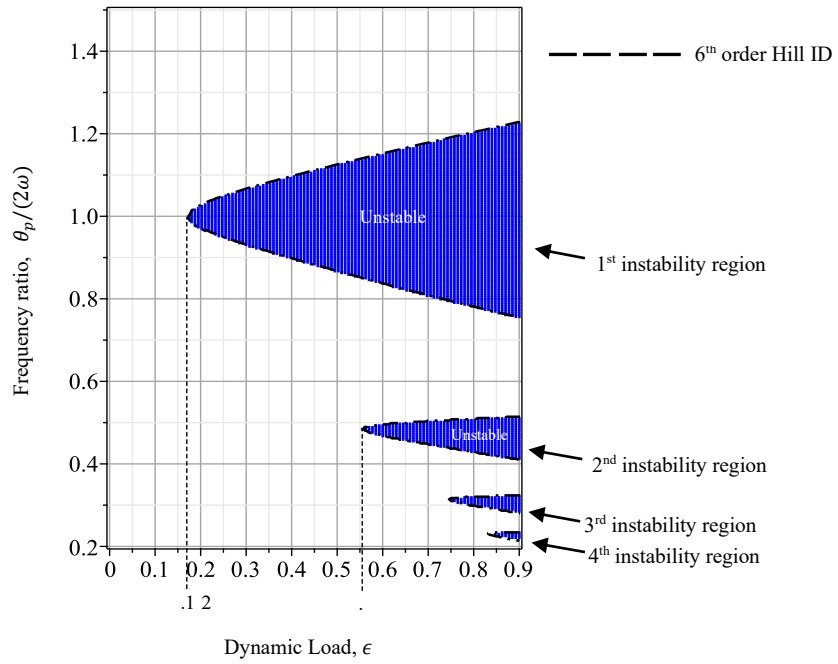
b)  $\epsilon = 0.4$   $\eta = 0.1$   $\delta = 0.3$ .



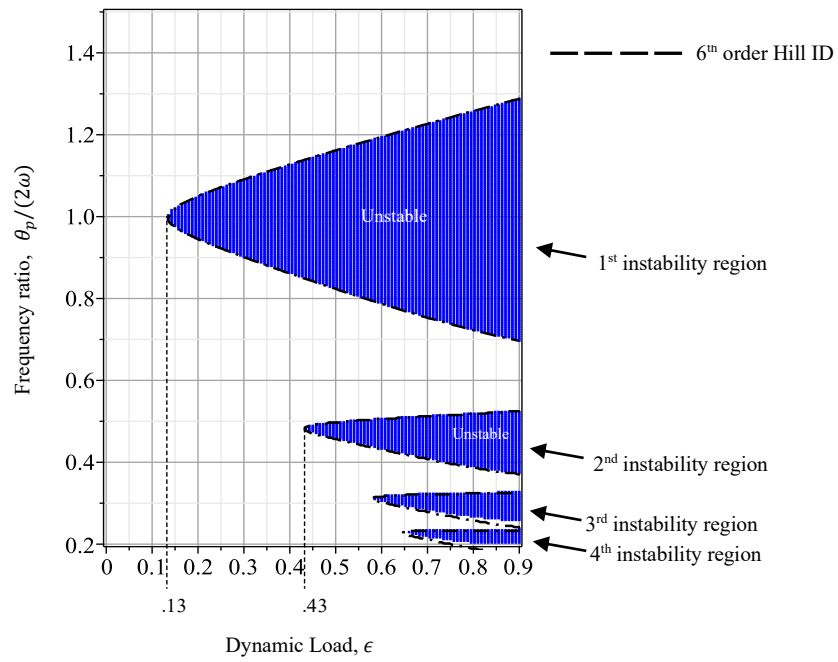
c)  $\epsilon = 0.6$   $\eta = 0.1$   $\delta = 0.3$ .

Figure 5.8 The static component weight impact.

The instability charts for several static stresses  $\lambda = 0.2, 0.4, 0.6$  are displayed in Figure 5.9. When the shifting load grows, the spectrum of the stimulation frequency for instability is enhanced almost linearly.



a)  $\lambda = 0.2$   $\eta = 0.1$   $\delta = 0.3$



b)  $\lambda = 0.4$   $\eta = 0.1$   $\delta = 0.3$

Fig. 5.9 The dynamic element load impact: (a)  $\lambda = 0.2$ ; (b)  $\lambda = 0.4$ ; (c)  $\lambda = 0.6$ .

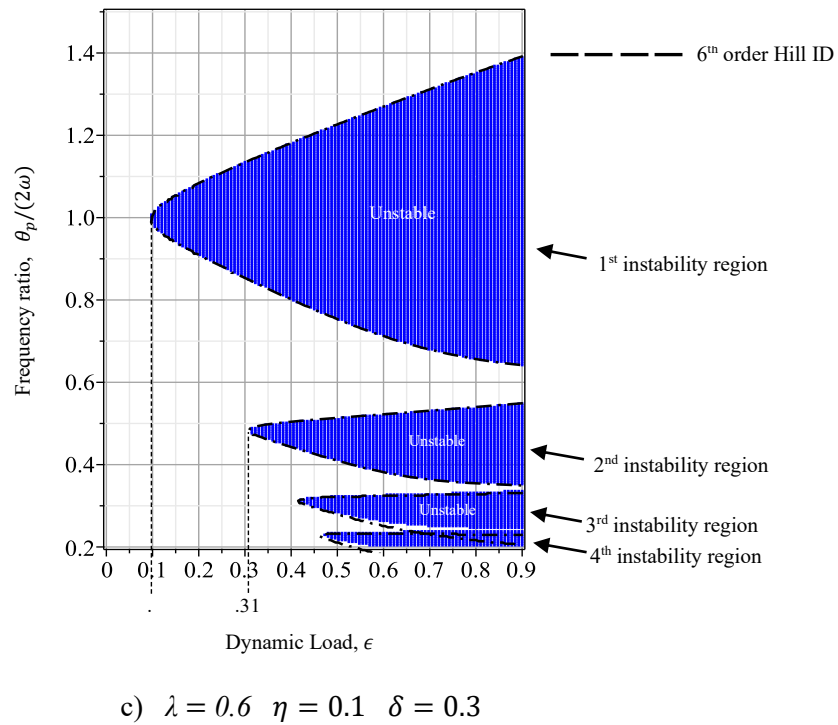


Fig. 5.9 The dynamic element load impact (Continued)

## 5.8 Summary

This chapter provides an in-depth exploration of dynamic instability regions in pile foundations by providing a case study, with a focus on seismic events. The chapter demonstrates how the Step Function method provides results comparable to the Harmonic Balance method, showcasing the accuracy of the computational modeling. Calibration of results from the Harmonic Balance method is also presented, emphasizing the identification of instability zones using Hill ID limitations. The chapter further explores the impact of parameters such as elastic foundation rigidity, damping, and dynamic and static loads on the instability regions. Theoretical discussions are complemented by detailed numerical simulations and stability diagrams, providing valuable insights into the dynamic behavior of pile foundations under various conditions.

## **Chapter 6 Conclusions and Recommendations**

### **6.1 Conclusions**

Pile foundations are crucial in civil engineering, transferring loads to soil and preventing structural failures that could lead to damage, collapse, or loss of life. Traditional studies focus on single-frequency dynamic forces, but there is a research gap regarding the effects of dual-frequency seismic excitations on pile stability. The main results of the thesis include:

#### **1. Driving Equation of Motion**

The beginning of this thesis is dedicated to intricately modeling pile foundations under dynamic loads, encompassing both single and dual frequencies. The central focus involves constructing a beam model supported by a Winkler foundation, incorporating a pair of frequencies. The derivation of the equation of motion utilizes equilibrium formulas and transforms a partial differential equation into an ordinary one through the Galerkin technique.

#### **2. Approximate Method - Harmonic Balance**

The third chapter shifts the exploration towards the investigation of the stability diagram of a pile foundation under dual-frequency dynamic loading. Utilizing the Harmonic Balance technique, the chapter employs Hill's infinite variables to formulate transition curves, revealing instabilities within the V-shaped region. This chapter stands as a substantial contribution to understanding pile foundation dynamics and the phenomena of instability under dual-frequency excitations.

By using the Hill infinite determinant, the Harmonic Balance method approach yields approximate stability and instability boundaries of different orders. In order to concurrently gain the dynamic stability and vibration reactions of piles on elastic bases using a single matrix procedure, an innovative computational simulation algorithm is proposed in this work.

#### **3. Numerical Method – Step Function**

Chapter four builds upon the step function method as a numerical method for investigating stability diagrams with dual frequency, first of all converting a two-frequency system into a Hill equation with a single primary frequency. It introduces a computational algorithm using step functions for the undamped Mathieu-Hill equation, providing insights into dynamic stability.

- The numerical method comprises two essential stages: (1) transforming the dual-frequency structure into a Hill formula featuring a solitary primary frequency, denoted as  $T_p$ ; (2) establishing a mathematical protocol specifically designed for analyzing the stability of motion characterized by a single frequency, which is called the Step Function Method.
- The research demonstrates that the suggested algorithm may generate precise and dependable outcomes, and it may be employed as well to evaluate the applicability of the traditional Harmonic Balance method. The different orders of Hill infinite factors from the Harmonic Balance method are calibrated using the computationally true stability charts. The second and third-order Hill ID boundaries are appropriate for the first instability zone, while the first-order Hill ID border is erroneous. The fourth-order Hill ID boundary is appropriate for the third instability zone, but neither the second-order nor the third-order Hill ID boundaries are precise. The fourth-order Hill ID border for the fifth instability zone is not precise.
- The first-order Hill ID limit for the second instability zone is erroneous and the second Hill ID borders lead to differences in the area's lower border, yet the third-order Hill ID boundaries are appropriate. The fourth-order Hill ID boundary is appropriate for the fourth instability zone, but neither the second-order nor the third-order boundaries are exact. The sixth instability zone cannot embrace the fourth-order limit.
- The vibration reactions, showing instability if growing substantially and stability if decreasing to rest, have validated the computational instability charts. Additionally, a comparison is made between the vibration reactions and the fourth-order Runge-Kutta method outcomes. It can be observed that the reliability of the current mathematical findings obtained from the method in Sect. 4 is equal to that of the Runge-Kutta method.
- The impact of loads on both static and dynamic components is investigated. The spectrum of the stimulation rate for instability grows substantially alongside a rise in static load. Both the essential dynamic load and the frequency of parametric resonance will decrease as the static stress increases. The spectrum of the stimulation rate for instability grows almost linearly with a boost in dynamic load.

- The current study of dynamic stability and reactions to vibration may shed light on the secure and efficient usage of piles on elastic foundations excited with two dynamic loads with different frequencies in mechanical and civil engineering fields. Relevant topics that will be covered in subsequent research are post-buckling and the nonlinearity of the pile. Yet when Mathieu-Hill formulas play a role, the suggested computational approach can be expanded to include dynamic stability and vibration assessment of numerous degrees of flexibility systems according to arbitrary parameterized stimulation.

The study primarily focuses on a beam model, with two key assumptions identified as limitations: first, the soil is represented as a single layer; second, the modeling uses a Winkler foundation model. The implications of this research are highly practical, particularly in the realm of designing pile foundations for megastructures. Designers can use the insights from this study to incorporate the effects of multiple frequencies on pile behavior into their design considerations, thereby enhancing the structural integrity and safety of constructions.

## **6.2 Recommendations for future research**

As with any scientific endeavor, we have limitations as same as this study opens several avenues for future research, which are essential to further advance this field.

Firstly, future studies could explore the extension of the numerical methods used in this research to more complex pile foundation systems, considering various soil types and pile materials. This expansion would provide a more comprehensive understanding of how different materials and soil conditions impact the dynamic stability of pile foundations in seismic environments. It would be particularly interesting to study the behavior of pile foundations in liquefiable soils, which present unique challenges during seismic events.

Another valuable area of research would involve the application of the findings from this study to the design and optimization of pile foundations for megastructures in seismically active regions. This would entail using the stability diagrams and response predictions developed in this thesis to enhance the structural integrity and safety of such constructions. Additionally, investigating the impact of multiple seismic frequencies on the dynamic behavior of other critical structures, such as bridges and high-rise buildings, would be beneficial.

## References

Ahuja, R., & Duffield, R. C. (1975). Parametric instability of variable cross-section beams resting on an elastic foundation. *Journal of Sound and Vibration*, 39(2), 159-174.

Bhattacharya, S., Adhikari, S., & Alexander, N. A. (2009). A simplified method for unified buckling and free vibration analysis of pile-supported structures in seismically liquefiable soils. *Soil Dynamics and Earthquake Engineering*, 29(8), 1220-1235.

Broer, H., & Simó, C. (1998). Hill's equation with quasi-periodic forcing: resonance tongues, instability pockets and global phenomena. *Boletim da Sociedade Brasileira de Matemática-Bulletin/Brazilian Mathematical Society*, 29(2), 253-293.

Byatt-Smith, J. G. (1979). DW Jordan and P. Smith, *Nonlinear Ordinary Differential Equations* (Oxford Applied Mathematics and Computing Series), 360 pp., *Proceedings of the Edinburgh Mathematical Society*, 22(1), 71-71.

Cong, Y., Kang, H., & Yan, G. (2021). Investigation of dynamic behavior of a cable-stayed cantilever beam under two-frequency excitations. *International Journal of Non-Linear Mechanics*, 129, 103670.

Deng, J. (2021). Analytical and numerical investigations on pillar rockbursts induced by triangular blasting waves. *International Journal of Rock Mechanics and Mining Sciences*, 138, 104518.

Deng, J. (2023a). Numerical simulation of stability and responses of dynamic systems under parametric excitation. *Applied Mathematical Modelling*, 2023: 119: 648-676

Deng, J. (2023b). Numerical investigation on stability of columns under dynamic loads with two frequencies. *COMPADYN 2023. 9th ECCOMAS Thematic Conference on Computational Methods in Structural Dynamics and Earthquake Engineering*. M. Papadrakakis, M. Fragiadakis (eds.), Greece:4451-4462.

Deng, J., Kanwar, N. S., Pandey, M. D., & Xie, W. C. (2019). Dynamic buckling mechanism of pillar rockbursts induced by stress waves. *Journal of Rock Mechanics and Geotechnical Engineering*, 11(5), 944-953.

Deng, J., Shahroudi, M., & Liu, K. (2023). Dynamic stability and responses of beams on elastic foundations under a parametric load. *International Journal of Structural Stability and Dynamics*, 23(02), 2350018.

Davis, S. H., & Rosenblat, S. (1980). A quasiperiodic Mathieu–Hill equation. *SIAM Journal on Applied Mathematics*, 38(1), 139-155.

Engel, R. S. (1991). Dynamic stability of an axially loaded beam on an elastic foundation with damping. *Journal of sound and vibration*, 146(3), 463-477.

Gabr, M. A., Wang, J. J., & Zhao, M. (1997). Buckling of piles with general power distribution of lateral subgrade reaction. *Journal of Geotechnical and Geoenvironmental Engineering*, 123(2), 123-130.

Gu, W., Yao, W., Shi, Y., Xie, L., Lian, X., Zhou, J., & Wen, X. (2022). Study on dynamic stability for the superlong pile foundation of marine engineering structures in service. *Institution of Structural Engineers, Elsevier*. (Vol. 41, pp. 1257-1265).

Iwatsubo, T., Saigo, M., & Sugiyama, Y. (1973). Parametric instability of clamped-clamped and clamped-simply supported columns under periodic axial load. *Journal of sound and vibration*, 30(1), 65-IN2.

Jimenez, G. A. L. (2019). *Static and Dynamic behaviour of pile supported structures in soft soil* (Doctoral dissertation, Université Grenoble Alpes).

Johnson, R., & Moser, J. (1982). The rotation number for almost periodic potentials. *Communications in Mathematical Physics*, 84(3), 403-438.

Lee, Joon Kyu. (2018). A unified model for analyzing free vibration and buckling of end-bearing piles. *Ocean Engineering, Elsevier*, 152 (2018): 17-25.

Liu, D. (2001). Dynamic stability analysis of frame systems by application of the finite element method. *Doctoral thesis*, University of Louisville, 2001.

Liu, J., Shao, X., Cheng, B., Cao, G., & Li, K. (2020). Study on buckling behavior of tapered friction piles in soft soils with linear shaft friction. *Advances in Civil Engineering*, 2020, 1-9.

Madabhushi, Gopal, Stuart Haigh, and Jonathan Knappett. (2009) *Design of pile*

*foundations in liquefiable soils*. World Scientific, 2009.

Magnus, W. and Winkler, S. (1966) *Hill's Equation*. John Wiley & Sons, New York.

Nayfeh, A. H., & Mook, D. T. (2008). *Nonlinear oscillations*. John Wiley & Sons.

Patil, M. A., & Kadoli, R. (2020). Influence of Winkler and viscoelastic foundation on free vibration of functionally graded beam integrated with Terfenol-D layer. *Journal of the Brazilian Society of Mechanical Sciences and Engineering*, 42(11), 591.

Prakash, Shamsher, and Hari D. Sharma. *Pile foundations in engineering practice*. John Wiley & Sons, 1991.

Puig, J., & Simó, C. (2011). Resonance tongues in the Quasi-Periodic Hill-Schrödinger Equation with three frequencies. *Regular and Chaotic Dynamics, Springer*, 16, 61-78.

Plaut, R. H., HaQuang, N., & Mook, D. T. (1986). Simultaneous resonances in non-linear structural vibrations under two-frequency excitation. *Journal of sound and vibration*, 106(3), 361-376.

Plaut, R. H., & Hsieh, J. C. (1985). Oscillations and instability of a shallow-arch under two-frequency excitation. *Journal of Sound and Vibration*, 102(2), 189-201.

Rand, R., & Hastings, R. (1995). A quasiperiodic Mathieu equation. In *International Design Engineering Technical Conferences and Computers and Information in Engineering Conference* (Vol. 17186, pp. 747-758). American Society of Mechanical Engineers.

Rand, R., Zounes, R., & Hastings, R. (1999). Dynamics of a quasiperiodically-forced Mathieu oscillator. In *IUTAM Symposium on New Applications of Nonlinear and Chaotic Dynamics in Mechanics: Proceedings of the IUTAM Symposium held in Ithaca, NY, USA, 27 July–1 August 1997* (pp. 61-70). Dordrecht: Springer Netherlands.

Richards, J. A. (1975). On the choice of steps in the piecewise-constant hill equation model of a quadrupole mass filter. *International Journal of Mass Spectrometry and Ion Physics*, 18(1), 11-19.

Rostami, R., Mickovski, S. B., Hytiris, N., & Bhattacharya, S. (2020). The Dynamic Behaviour of Pile Foundations in Seismically Liquefiable Soils: Failure Mechanisms, Analysis, Re-Qualification. In *Earthquakes-From Tectonics to Buildings*. IntechOpen.

Sahoo, B., Panda, L. N., & Pohit, G. (2016). Combination, principal parametric and internal resonances of an accelerating beam under two frequency parametric excitation. *International Journal of Non-Linear Mechanics*, 78, 35-44.

Shahroudi, M. (2023). *Dynamic Stability of Piles Under Earthquake With Fractional Damping Foundation* (master's dissertation), Lakehead University.

Shan, Y., Ma, W., Xiang, K., Wang, B., Zhou, S., & Guo, H. (2022). Vertical dynamic response of a floating pile in unsaturated poroelastic media based on the fictitious unsaturated soil pile model. *Applied Mathematical Modelling*, 109, 209-228.

Sharma, A., & Sinha, S. C. (2018). An approximate analysis of quasi-periodic systems via Floquet theory. *Journal of Computational and Nonlinear Dynamics*, 13(2), 021008.

Stringer, M. E. (2012). The axial behaviour of piled foundations in liquefiable soils. (Doctoral dissertation, University of Cambridge).

Tanahashi, H., & Suzuki, Y. (2020). Review on the mechanical models and formulations of embedment of traditional timber joints in Japan. *Japan Architectural Review*, 3(2), 148-164.

Udo-Akpan, A.M. (2018). On The Buckling Modes and Static Buckling Of a Column Lying On Nonlinear Elastic Foundations but With One End Simply-Supported While the Other End Is Clamped. *IOSR Journal of Mathematics (IOSR-JM)*, 14, 16-23.

Wang, J., Lo, S. H., & Zhou, D. (2014). Effect of a forced harmonic vibration pile to its adjacent pile in layered elastic soil with double-shear model. *Soil Dynamics and Earthquake Engineering*, 67, 54-65.

Waters, T. J. (2010). Stability of a 2-dimensional Mathieu-type system with quasiperiodic coefficients. *Nonlinear dynamics*, 60, 341-356.

Xie, W. C. (2006). *Dynamic stability of structures*. Cambridge University Press.

Yang, J., & Ye, J. Q. (2002). Dynamic elastic local buckling of piles under impact loads. *Structural engineering and mechanics: An international journal*, 13(5), 543-556.

Yao, W., & Shi, Y. (2022). Dynamic stability analysis of pile groups under wave

---

load. *Applied Mathematical Modelling*, 110, 367-386.

Yokoyama, T. (1988). Parametric instability of Timoshenko beams resting on an elastic foundation. *Computers & structures*, 28(2), 207-216.

Zhang, D., Tang, Y., Liang, R., Song, Y., & Chen, L. (2022). Internal resonance of an axially transporting beam with a two-frequency parametric excitation. *Applied Mathematics and Mechanics*, 43(12), 1805-1820.

Zhang, D., Tang, Y., Liang, R., Yang, L., & Chen, L. Q. (2021). Dynamic stability of an axially transporting beam with two-frequency parametric excitation and internal resonance. *European Journal of Mechanics-A/Solids*, 85, 104084.

Zhao, Y., Huang, C., Chen, L., & Peng, J. (2018). Nonlinear vibration behaviors of suspended cables under two-frequency excitation with temperature effects. *Journal of Sound and Vibration*, 416, 279-294.

Zounes, R. S. (1997). *An analysis of the nonlinear quasiperiodic Mathieu equation*. Cornell University.

Zounes, R. S., & Rand, R. H. (1998). Transition curves for the quasi-periodic Mathieu equation. *SIAM Journal on Applied Mathematics*, 58(4), 1094-1115.